

1 **Temporary and net sinks of atmospheric CO₂ due to chemical**
2 **weathering in subtropical catchment with mixing carbonate and**
3 **silicate lithology**

4 Yingjie Cao^{a,c,d}, Yingxue Xuan^{a,b}, Changyuan Tang^{a,b,c*}, Shuai Guan^e, Yisheng Peng^{a,c}

5 ^aSchool of Environmental Science and Engineering, Sun Yat-Sen University, Guangzhou,
6 China

7 ^bSchool of Geography and Planning, Sun Yat-Sen University, Guangzhou, China

8 ^cGuangdong Provincial Key Laboratory of Environmental Pollution Control and Remediation
9 Technology, Sun Yat-Sen University, Guangzhou, China

10 ^dSouthern Marine Science and Engineering Guangdong Laboratory, Zhuhai, China

11 ^eGuangdong Research Institute of Water Resource and Hydropower, Guangzhou, China

12
13 **Abstract:** The study provided the major ion chemistry, chemical weathering rates and temporary
14 and net CO₂ sinks in the Beijiang River, which was characterized as hyperactive region with high
15 chemical weathering rates, carbonate and silicate mixing lithology and abundant sulfuric acid
16 chemical weathering agent of acid deposition and acid mining drainage (AMD) origins. The total
17 chemical weathering rate of 85.46 t·km⁻²·a⁻¹ was comparable to other rivers in the hyperactive zones
18 between the latitude 0-30°. Carbonate weathering rate of 61.15 t·km⁻²·a⁻¹ contributed to about 70%
19 of the total. The lithology, runoff and geomorphology had significant influence on the chemical
20 weathering rate. The proportion of carbonate outcrops had significant positive correlation with the
21 chemical weathering rate. Due to the interaction between dilution and compensation effect,
22 significant positive linear relationship was detected between runoff and total, carbonate and silicate

23 weathering rates. The geomorphology factors such as catchment area, average slope and
24 hypsometric integral value (HI) had non-linear correlation with chemical weathering rate and
25 showed significant scale effect, which revealed the complexity in chemical weathering processes.
26 DIC-apportionment showed that CCW (Carbonate weathering by CO₂) was the dominant origin of
27 DIC (35%-87%). SCW (Carbonate weathering by H₂SO₄) (3%-15%) and CSW (Silicate weathering
28 by CO₂) (7%-59%) were non-negligible processes. The temporary CO₂ sink was 823.41 10³ mol
29 km⁻² a⁻¹. Compared with the “temporary” sink, the net sink of CO₂ for the Beijiang River was
30 approximately 23.18×10³ mol km⁻² a⁻¹ of CO₂ and was about 2.82% of the “temporary” CO₂ sink.
31 Human activities (sulfur acid deposition and AMD) dramatically decreased the CO₂ net sink and
32 even make chemical weathering a CO₂ source to the atmosphere.

33 **Keywords:** Chemical weathering, DIC-apportionment, CO₂ temporary sink, CO₂ net sink

34 **1 Introduction**

35 Chemical weathering driven by weak carbonic acid (H₂CO₃) that originates from atmosphere
36 CO₂ or soil respiration under natural conditions is a fundamental geochemical process regulating
37 the atmosphere-land-ocean carbon fluxes and earth’s climate (Guo et al., 2015). Carbonate and
38 silicate weathering define the two typical categories of chemical weathering. From the view of the
39 global carbon cycle, the CO₂ consumption due to carbonate weathering is recognized the “temporary”
40 sink because the flux of CO₂ consumed by carbonate dissolution on the continents is balanced by
41 the flux of CO₂ released into the atmosphere from the oceans by carbonate precipitation on the
42 geological time scale (Cao et al., 2015; Garrels, 1983). While the consumption of CO₂ during the
43 chemical weathering of silicate rocks has been regard as the net sink of CO₂ and regulates the global
44 carbon cycle (Hartmann et al., 2009; Hartmann et al., 2014b; Kempe and Degens, 1985; Lenton and

45 Britton, 2006). Thus in carbonate-silicate mixing catchment, it is essential to distinguish proportions
46 of the two most important lithological groups, i.e., carbonates and silicates, and evaluate the net
47 CO₂ sink due to chemical weathering of silicate (Hartmann et al., 2009).

48 In addition to the chemical weathering induced by H₂CO₃, sulfuric acid (H₂SO₄) of
49 anthropogenic origins produced by sulfide oxidation such as acid deposition caused by fossil fuel
50 burning and acid mining discharge (AMD) also becomes an important chemical weathering agent
51 in the catchment scale. Many studies have shown the importance of sulfide oxidation and subsequent
52 dissolution of other minerals by the resulting sulfuric acid at catchment scale (Hercod et al., 1998;
53 Spence and Telmer, 2005). Depending on the fate of sulfate in the oceans, sulfide oxidation coupled
54 with carbonate dissolution could facilitate a release of CO₂ to the atmosphere (Spence and Telmer,
55 2005), the carbonate weathering by H₂SO₄ plays a very important role in quantifying and validating
56 the ultimate CO₂ consumption rate. Thus, under the influence of human activities, the combination
57 of silicate weathering by H₂CO₃ and carbonate weathering by H₂SO₄ controlled the net sink of
58 atmospheric CO₂.

59 Numerous studies on chemical weathering of larger rivers have been carried out to examine
60 hydrochemical characteristics, chemical erosion and CO₂ consumption rates, and long-term climatic
61 evolution of the Earth, such as the Changjiang River (Chen et al., 2002; Ran et al., 2010), the
62 Huanghe River (Zhang et al., 1995), the Pearl River (Gao et al., 2009; Xu and Liu, 2010; Zhang et
63 al., 2007), the Huai River (Zhang et al., 2011), the rivers of the Qinghai-Tibet Plateau (Jiang et al.,
64 2018; Li et al., 2011; Wu et al., 2008), the Mekong River (Li et al., 2014), the rivers of the Alpine
65 region (Donnini et al., 2016), the Sorocabá River (Fernandes et al., 2016), the rivers of Baltic Sea
66 catchment (Sun et al., 2017), the Amazon River (Gibbs, 1972; Mortatti and Probst, 2003; Stallard

67 and Edmond, 1981; Stallard and Edmond, 1983; Stallard and Edmond, 1987), the Lena River (Huh
68 and Edmond, 1999) and the Orinoco River (Mora et al., 2010). For simplicity of calculation
69 procedure, most of the researches have ignored the sulfuric acid induced chemical weathering and
70 resulted in an overestimation of CO₂ sink. To overcome this shortcoming of traditional mass-balance
71 method, we applied a DIC source apportionment procedure to discriminate the contribution of
72 sulfuric acid induced chemical weathering to validate the temporary and net sink of CO₂ in a typical
73 hyperactive region with carbonate-silicate mixing lithology to give a further understanding of basin
74 scale chemical weathering estimation.

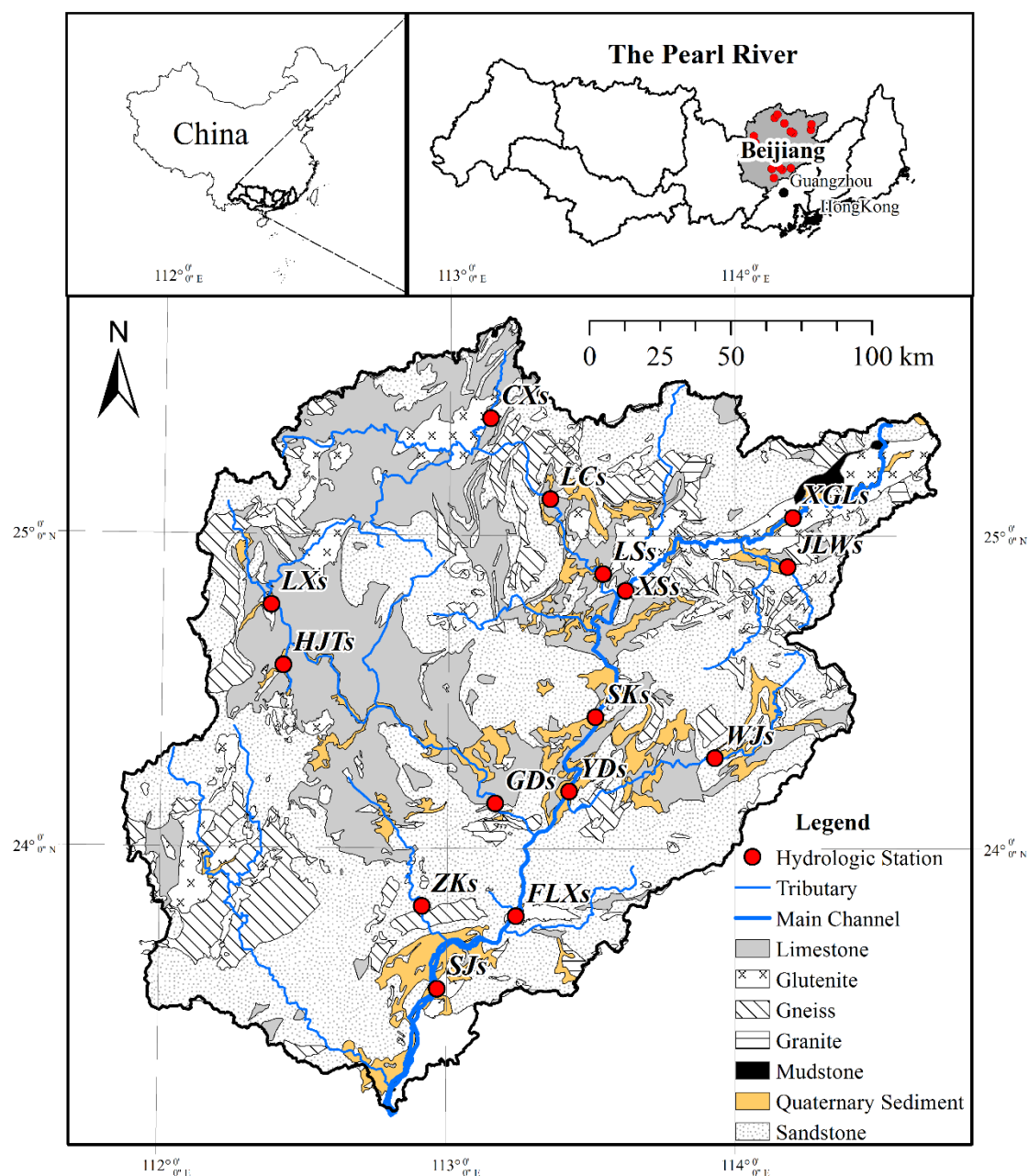
75 About half of the global CO₂ sequestration due to chemical weathering occurs in warm and
76 high runoff regions (Ludwig et al., 1998), so called the hyperactive regions and hotspots (Meybeck
77 et al., 2006). The Pearl River located in the subtropical area in South China includes three principal
78 rivers: the Xijiang, Beijiang, and Dongjiang Rivers. The warm and wet climatic conditions make
79 the Pearl River a hyperactive region in China. The three river basins have distinct geological
80 conditions. The Xijiang River is characterized as the carbonate-dominated area and the Dongjiang
81 River has silicate as the main rock type. While the Beijiang River, which is the second largest
82 tributary of the Pearl River, is characterized as a typical carbonate-silicate mixing basin. In addition,
83 as the serve acid deposition (Larssen et al., 2006) and active mining area (Li et al., 2019), chemical
84 weathering induced by sulfuric acid make the temporary and net sink of atmospheric CO₂ to be
85 reevaluated. So that, in this study, the Beijiang River in Southeast China with a typical subtropical
86 monsoon climate and carbonate-silicate mixing geologic settings was selected as the study area.
87 Three main objectives were summarized as follows: (1) revealed spatial-temporal variations of
88 major element chemistry of the river water, (2) calculated the chemical weathering rate and

89 unraveled the controlling factors on chemical weathering processes, and (3) determined the
90 temporary sink of CO₂ and evaluated the influence of sulfide oxidation on net sink of CO₂ by DIC
91 apportionment procedure.

92 **2 Study area**

93 The Beijiang River Basin, which is the second largest tributary of the Pearl River Basin, is
94 located in the southeast of China (Fig. 1). It covers an area of 52 068 km² and has a total length of
95 573 km. The river basin is located in subtropical monsoon climate zone, with the mean annual
96 temperature across the drainage basin ranging from 14°C to 22°C, the mean annual precipitation
97 ranging from 1390 mm to 2475 mm. The average annual runoff is 51 billion m³, with 70%-80% of
98 the flux occurring from April to September. This can be attributed to the fact that more than 70% of
99 the annual precipitation (about 1800 mm year⁻¹) is concentrated in the wet season (April to
100 September).

101 Lithology in the river basin is composed of limestone, sandstone, gneiss and glutenite. In the
102 upper basin, carbonate rock (mainly of limestone) outcrops in the west and center, while sandstone
103 of Devonian era and mudstone of Paleogene era outcrop in the east of upper stream. In the middle
104 of basin, limestone and sandstone cover most of the area, and Cretaceous volcanic rocks are found
105 in the tributary (Lianjiang River), mainly granite. In the lower basin, Achaen metamorphic rocks
106 outcrop in the west, and are composed of gneiss and schist, sandstone covers rest of area of the
107 lower basin. Quaternary sediments scatter along the main stream of the river. The carbonate and
108 silicate rock outcrops in the Beijiang River Basin was 10737 km² (28%) and 24687 km² (65%),
109 respectively.



110
111 **Fig. 1 Geology map and sampling point in the Beijiang River basin by ArcGis**

112 **3 Materials and methods**

113 **3.1 Sampling procedure and laboratory analysis**

114 Water samples were collected monthly at 15 hydrologic stations from January to December in
115 2015 (Fig. 1). The river waters were sampled by a portable organic class water sampler along the
116 middle thread of channel in the first day of each month. In addition, to discriminate the contribution
117 of rain inputs, the daily rainwater was also sampled in five stations (SJs, FLXs, YDs, XSs and XGLs)

118 along the main stream. The rainwater collector is consisted of a funnel with diameter of 20 cm and
119 a 5 L plastic bottle. A rubber ball is setup in the funnel to prevent evaporation. All the river and rain
120 water were filtered through 0.45 μm glass fiber filter and stored in 100 ml tubes and stored below
121 4°C until analysis.

122 Electric conductivity (EC), pH and temperature (T) were measured by a multi-parameter water
123 quality meter (HACH-HQ40Q), and alkalinity (HCO_3^-) was measured in filtered water samples by
124 titration in situ. The dissolved SiO_2 was measured by molybdenum yellow method and was analyzed
125 by ultraviolet spectrophotometer (Shimadzu UV-2600). The cations (Na^+ , K^+ , Ca^{2+} , Mg^{2+}) and
126 anions (Cl^- , SO_4^{2-}) were analyzed by ion chromatography (ThermoFisher ICS-900) with limit of
127 detection (L.O.D) of 0.01 mg/L. Reference, blank and replicate samples were employed to check
128 the accuracy of all the analysis and the relative standard deviations of all the analysis were within
129 $\pm 5\%$. The electrical balance (E.B.) defined by the equation of $\text{E.B.} =$
130 $\frac{\text{meq}(\text{sum of cations}) - \text{meq}(\text{sum of anions})}{\text{meq}(\text{sum of cations and anions})} \times 100$ of the water samples was less than 5%.

131 3.2 Calculation procedure

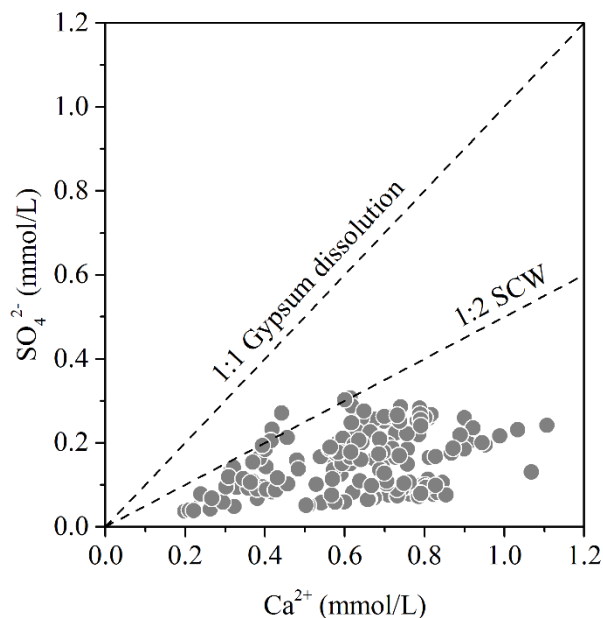
132 3.2.1 Chemical weathering rates

133 The mass balance equation for element X in the dissolved load can be expressed as (Galy and
134 France-Lanord, 1999):

$$135 \quad [X]_{\text{riv}} = [X]_{\text{pre}} + [X]_{\text{eva}} + [X]_{\text{sil}} + [X]_{\text{car}} + [X]_{\text{anth}} \quad (1)$$

136 Where $[X]$ denotes the elements of Ca^{2+} , Mg^{2+} , Na^+ , K^+ , Cl^- , SO_4^{2-} , HCO_3^- in $\text{mmol}\cdot\text{L}^{-1}$. The
137 subscripts riv, pre, eva, sil, car and anth denote the river, precipitation source, evaporite source,
138 silicate source, carbonate source and anthropogenic source. The hydrochemical compositions of rain
139 water were summarized in Table S1 in the supplementary materials.

140 In the study area, the anthropogenic source of major ions **except for** SO_4^{2-} was ignored due to
141 the following two reasons. (1) Two main characteristics of much polluted rivers are that TDS is
142 greater than 500 mg/L and the Cl^-/Na^+ molar ratio is greater than that of sea salts (about 1.16) (Cao
143 et al., 2016a; Gaillardet et al., 1999). The TDS in the study area ranged from 73.79 to 230.16 $\text{mg}\cdot\text{L}^{-1}$
144 and the low TDS implied that the anthropogenic origins of major ions could be ignored in the study.
145 However, the Beijiang River is characterized as a typical region suffered from severe acid deposition
146 (Larsen et al., 2006) and active mining area (Li et al., 2019). The acid deposition and acid mining
147 discharge contribute to the highest concentration of SO_4^{2-} . (2) Natural origin of SO_4^{2-} is the
148 dissolution of evaporite, such as gypsum, while no evaporite was found in the study area. If SO_4^{2-}
149 comes from the gypsum dissolution, the ratios of Ca^{2+} and SO_4^{2-} should be close to 1:1. The
150 stoichiometric analysis (Fig.2) showed that the ratio of Ca^{2+} and SO_4^{2-} deviated from 1:1 and also
151 proved this point.



152
153 **Fig. 2 Stoichiometric relationship between Ca^{2+} and SO_4^{2-} . The “SCW” means carbonate**
154 **weathering induced by sulfuric acid**

155 So that, on the basis of the theory of rock chemical weathering and ignoring the anthropogenic

156 origins of major ions (except for SO_4^{2-}), the major elements of river water can be simplified as

157 followed:

$$158 \quad [\text{Cl}^-]_{\text{riv}} = [\text{Cl}^-]_{\text{pre}} + [\text{Cl}^-]_{\text{eva}} \quad (2)$$

$$159 \quad [\text{K}^+]_{\text{riv}} = [\text{K}^+]_{\text{pre}} + [\text{K}^+]_{\text{sil}} \quad (3)$$

$$160 \quad [\text{Na}^+]_{\text{riv}} = [\text{Na}^+]_{\text{pre}} + [\text{Na}^+]_{\text{eva}} + [\text{Na}^+]_{\text{sil}} \quad (4)$$

$$161 \quad [\text{Ca}^{2+}]_{\text{riv}} = [\text{Ca}^{2+}]_{\text{pre}} + [\text{Ca}^{2+}]_{\text{sil}} + [\text{Ca}^{2+}]_{\text{car}} \quad (5)$$

$$162 \quad [\text{Mg}^{2+}]_{\text{riv}} = [\text{Mg}^{2+}]_{\text{pre}} + [\text{Mg}^{2+}]_{\text{sil}} + [\text{Mg}^{2+}]_{\text{car}} \quad (6)$$

$$163 \quad [\text{HCO}_3^-]_{\text{sil}} = [\text{K}^+]_{\text{sil}} + [\text{Na}^+]_{\text{sil}} + 2[\text{Mg}^{2+}]_{\text{sil}} + 2[\text{Ca}^{2+}]_{\text{sil}} \quad (7)$$

$$164 \quad [\text{HCO}_3^-]_{\text{car}} = [\text{HCO}_3^-]_{\text{riv}} - [\text{HCO}_3^-]_{\text{sil}} \quad (8)$$

$$165 \quad [\text{SO}_4^{2-}]_{\text{riv}} = [\text{SO}_4^{2-}]_{\text{pre}} + [\text{SO}_4^{2-}]_{\text{anth}} \quad (9)$$

166 Firstly, the measured ion concentrations of the rain water are rectified by evaporation

167 coefficient $\alpha=0.63=P/R$ (with P the precipitation and R the runoff) and calculated the contributions

168 of atmospheric precipitation. Secondly, the molar ratios of $\text{Ca}^{2+}/\text{Na}^+$ (0.4) and $\text{Mg}^{2+}/\text{Na}^+$ (0.2) for

169 silicate end-member (Zhang et al., 2007) are used to calculate the contribution of Ca^{2+} and Mg^{2+}

170 from silicate weathering, and then, residual Ca^{2+} and Mg^{2+} were attributed to carbonate weathering.

171 For monthly data, the contributions of different sources can be calculated as followed:

$$172 \quad R_{\text{car}} = ([\text{Ca}^{2+}]_{\text{car}} + [\text{Mg}^{2+}]_{\text{car}}) / S \times 100\% \quad (10)$$

$$173 \quad R_{\text{sil}} = ([\text{K}^+]_{\text{sil}} + [\text{Na}^+]_{\text{sil}} + [\text{Ca}^{2+}]_{\text{sil}} + [\text{Mg}^{2+}]_{\text{sil}}) / S \times 100\% \quad (11)$$

$$174 \quad R_{\text{eva}} = [\text{Na}^+]_{\text{eva}} / S \times 100\% \quad (12)$$

$$175 \quad R_{\text{pre}} = ([\text{K}^+]_{\text{pre}} + [\text{Na}^+]_{\text{pre}} + [\text{Ca}^{2+}]_{\text{pre}} + [\text{Mg}^{2+}]_{\text{pre}}) / S \times 100\% \quad (13)$$

$$176 \quad S = [\text{Ca}^{2+}]_{\text{car}} + [\text{Mg}^{2+}]_{\text{car}} + [\text{Ca}^{2+}]_{\text{sil}} + [\text{Mg}^{2+}]_{\text{sil}} + [\text{Na}^+]_{\text{sil}} + [\text{K}^+]_{\text{sil}} + [\text{Na}^+]_{\text{eva}} +$$

$$177 \quad [\text{Ca}^{2+}]_{\text{pre}} + [\text{Mg}^{2+}]_{\text{pre}} + [\text{Na}^+]_{\text{pre}} + [\text{K}^+]_{\text{pre}} \quad (14)$$

178 Where R denotes the proportions of dissolved cations from different sources. S denotes the total
 179 concentrations of cations for river water in $\text{mmol}\cdot\text{L}^{-1}$.

180 The total, carbonate and silicate chemical weathering rates (TWR, CWR and SWR) of a year
 181 can be estimated as followed:

$$182 \quad \text{CWR} = \sum_{i=1}^{n=12} [(24 \times [\text{Mg}^{2+}]_{\text{car}} + 40 \times [\text{Ca}^{2+}]_{\text{car}} + 61 \times [\text{HCO}_3^-]_{\text{car}} \times 0.5) \times Q_i / (10^6 A)] \quad (15)$$

$$183 \quad \text{SWR} = \sum_{i=1}^{n=12} [(39 \times [\text{K}^+]_{\text{sil}} + 23 \times [\text{Na}^+]_{\text{sil}} + 24 \times [\text{Mg}^{2+}]_{\text{sil}} + 40 \times [\text{Ca}^{2+}]_{\text{sil}} + 96 \times [\text{SiO}_2]_{\text{sil}}) \times$$

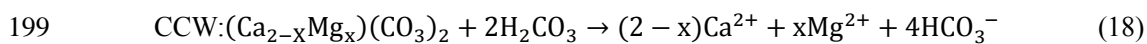
$$184 \quad Q_i / (10^6 A)] \quad (16)$$

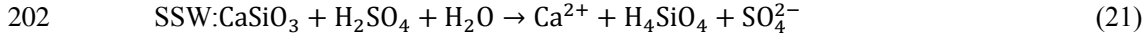
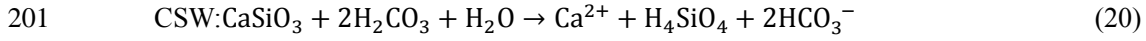
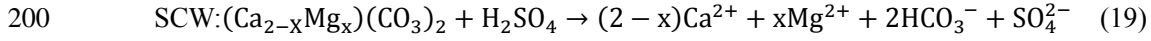
$$185 \quad \text{TWR} = \text{CWR} + \text{SWR} \quad (17)$$

186 Where TWR, CWR and SWR have the unit of $\text{t km}^{-2} \text{ a}^{-1}$, Q_i denotes discharge in $\text{m}^3 \cdot \text{month}^{-1}$, and A
 187 denotes the catchment area in km^2 .

188 3.2.2 DIC apportionments

189 In the Beijiing River, the pH values of water samples ranged from 7.5 to 8.5 with an average
 190 of 8.05. Under this pH conditions, the major species of DIC is HCO_3^- . In addition, HCO_3^- accounted
 191 for more than 95% in all sampling sites based on calculation, thus the concentration of HCO_3^-
 192 (mmol/L) was used to represent the DIC concentration in this study. The riverine DIC originates
 193 from several sources including carbonate minerals, respired soil CO_2 and atmospheric CO_2 , and it
 194 could be affected by processes occurring along the water pathways (Khadka et al., 2014; Li et al.,
 195 2008). Four dominant weathering processes, including (1) carbonate weathering by carbonic acid
 196 (CCW), (2) carbonate weathering by sulfuric acid (SCW), (3) silicate weathering by carbonic acid
 197 (CSW), (4) and silicate weathering by sulfuric acid (SSW), can be described by the following
 198 reaction equations:





203 Where CaSiO_3 represents an arbitrary silicate.

204 According to the study of Galy and France-Lanord (1999) and Spence and Telmer (2005),
 205 carbonate and silicate weathering by carbonic acid in the same ratio as carbonate and silicate
 206 weathering by sulfuric acid, for monthly data the mass balance equations are followed:

207 $[\text{SO}_4^{2-}]_{\text{riv}} - [\text{SO}_4^{2-}]_{\text{pre}} = [\text{SO}_4^{2-}]_{\text{SCW}} + [\text{SO}_4^{2-}]_{\text{SSW}}$ (22)

208 $[\text{SO}_4^{2-}]_{\text{riv}} - [\text{SO}_4^{2-}]_{\text{pre}} = \alpha_{\text{SCW}} \times [\text{HCO}_3^-]_{\text{riv}} \times 0.5 + \frac{\alpha_{\text{CSW}} \times \alpha_{\text{SCW}}}{\alpha_{\text{CCW}}} \times [\text{HCO}_3^-]_{\text{riv}}$ (23)

209 Where the subscripts CCW, SCW, CSW and SSW denotes the four end-members defined by
 210 carbonate weathering by carbonic acid, carbonate weathering by sulfuric acid, silicate weathering
 211 by carbonic acid and silicate weathering by sulfuric acid, respectively. The parameter α denotes the
 212 proportion of DIC derived from each end-member processes.

213 According to the above description, the ion balance equations are followed:

214 $[\text{Ca}^{2+}]_{\text{car}} + [\text{Mg}^{2+}]_{\text{car}} = \alpha_{\text{CCW}} \times [\text{HCO}_3^-]_{\text{riv}} \times 0.5 + \alpha_{\text{SCW}} \times [\text{HCO}_3^-]_{\text{riv}}$ (24)

215 $[\text{SO}_4^{2-}]_{\text{SCW}} + [\text{SO}_4^{2-}]_{\text{SSW}} = \alpha_{\text{SCW}} \times [\text{HCO}_3^-]_{\text{riv}} \times 0.5 + \frac{\alpha_{\text{CSW}} \times \alpha_{\text{SCW}}}{\alpha_{\text{CCW}}} \times [\text{HCO}_3^-]_{\text{riv}}$ (25)

216 $\alpha_{\text{CCW}} + \alpha_{\text{SCW}} + \alpha_{\text{CSW}} = 1$ (26)

217 Combing the above equations, the proportions of HCO_3^- derived from three end-members
 218 (CCW, SCW and CSW) can be calculated, and the DIC (equivalent to HCO_3^-) fluxes by different
 219 chemical weathering processes are calculated by following equations.

220 $[\text{HCO}_3^-]_{\text{CCW}} = \alpha_{\text{CCW}} \times [\text{HCO}_3^-]_{\text{riv}}$ (27)

221 $[\text{HCO}_3^-]_{\text{SCW}} = \alpha_{\text{SCW}} \times [\text{HCO}_3^-]_{\text{riv}}$ (28)

$$[HCO_3^-]_{CSW} = \alpha_{CSW} \times [HCO_3^-]_{riv} \quad (29)$$

3.2.3 CO₂ consumption rate and CO₂ net sink

According to the equations (17)~(20), only the processes of CCW and CSW can consume the CO₂ from atmosphere or soil and only half of the HCO₃⁻ in the water due to carbonate weathering by carbonic acid come from atmospheric CO₂. Thus, the CO₂ consumption rates (CCR) for CCW and CSW can be calculated as followed (Zeng et al., 2016):

$$CCR_{CCW} = \sum_{i=1}^{n=12} \{ [0.5 \times (Q/A) \times [HCO_3^-]_{CCW}] / 1000 \}_i \quad (30)$$

$$CCR_{CSW} = \sum_{i=1}^{n=12} \{ [(Q/A) \times [HCO_3^-]_{CSW}] / 1000 \}_i \quad (31)$$

Where Q is discharge in m³·a⁻¹, [HCO₃⁻] is concentration of HCO₃⁻ in mmol·L⁻¹, A is catchment area in km², so that the CCR has the unit of 10³ mol km⁻²·a⁻¹.

According to the classical view of the global carbon cycling (Berner and Kothavala, 2001), the CCW is not a mechanism that can participate to the amount of CO₂ in the atmosphere because all of the atmospheric fixed through CCW is returned to the atmosphere during carbonate precipitation in the ocean. However, when sulfuric acid is involved as a proton donor in carbonate weathering, half of the dissolved carbon re-release to the atmospheric during carbonate precipitation. Thus, SCW leads to a net release of CO₂ in ocean-atmosphere system over timescale typical of residence time of HCO₃⁻ in the ocean (10⁵ years). Meanwhile, in case of CSW, followed by carbonate deposition, one of the two moles of CO₂ involved is transferred from the atmosphere to the lithosphere in the form of carbonate rocks, while the other one returns to the atmosphere, resulting a net sink of CO₂. Therefore, the net CO₂ consumption rate (CCR_{Net}) due to chemical weathering can be concluded as followed:

$$CCR_{Net} = \sum_{i=1}^{n=12} \{ [(0.5 \times [HCO_3^-]_{CSW} - 0.5 \times [HCO_3^-]_{SCW}) \times (Q/A)] / 1000 \}_i \quad (32)$$

244 3.3 Spatial and statistical analysis

245 The hypsometric integral value (HI) (PIKE and WILSON, 1971) was employed in this study
246 to evaluate the influence of terrain on the chemical weathering. HI is an important index to reveal
247 the relationship between morphology and development of landforms and can be used to establish
248 the quantitative relationship between the stage of geomorphological development and the material
249 migration in the basin (PIKE and WILSON, 1971; Singh et al., 2008; STRAHLER, 1952). The HI
250 value of each watershed is calculated by the elevation-relief ratio method and can be obtained by
251 the following equation (PIKE and WILSON, 1971):

$$252 \quad HI = \frac{\text{Mean.elevation} - \text{Min.elevation}}{\text{Max.elevation} - \text{Min.elevation}} \quad (33)$$

253 Where HI is the hypsometric integral; Mean.elevation is the mean elevation of the watershed;
254 Min.elevation is the minimum elevation within the watershed; Max.elevation is the maximum
255 elevation within the watershed. According to the hypsometric integral value (HI), the
256 geomorphological development can be divided into three stages: inequilibrium or young stage (HI >
257 0.6), equilibrium or mature stage (0.35 < HI ≤ 0.6), and monadnock or old age (HI ≤ 0.35),
258 which can reflect the erodible degree and erosion trend of the geomorphology (Xiong et al., 2014).

259 The watershed of the study area was divided by using hydrological analysis module of ArcGIS.
260 The average slope and HI was conducted by spatial analysis module of ArcGIS. The area of
261 silicate/carbonate outcrops was calculated by hydrological module of ArcGIS based on geology map
262 from provided by China Geological Survey. The data of river water discharge was provided by the
263 local hydrology bureau.

264 All statistical tests were conducted using SPSS version 22.0. One-way analysis of variance
265 (ANOVA) was performed to check the differences of monthly major ion concentrations and

266 dissolved inorganic carbonate isotopes with significance at $p < 0.05$. Principal component analysis
267 (PCA) was employed to unravel the underlying data set through the reduced new variables, analyzed
268 the significant factors affecting the characteristics of water chemistry.

269 **4 Results**

270 **4.1 Chemical compositions**

271 The major physical-chemical parameters of river water samples were presented in Table 1. In
272 Table 1, the chemical parameters of river water were the flow-weighted average over 12 months.
273 For every sampling station, the flow-weighted average of ion concentration can be expressed
274 followed the equation $[X]_{average} = \frac{\sum_{i=1}^{n=12} [X]_i \times Q_i}{\sum_{i=1}^{n=12} Q_i}$, where $[X]$ denotes the elements of Ca^{2+} , Mg^{2+} ,
275 Na^+ , K^+ , Cl^- , SO_4^{2-} , HCO_3^- in $\text{mmol} \cdot \text{L}^{-1}$. Q denotes average monthly discharge in $\text{m}^3 \cdot \text{s}^{-1}$. The
276 subscripts i denotes 12 months from January to December. For all the monthly samples, the pH
277 values ranged from 7.5 to 8.5 with an average of 8.05. Average EC was $213 \mu\text{s} \cdot \text{cm}^{-1}$, ranging from
278 81 to $330 \mu\text{s} \cdot \text{cm}^{-1}$. The TDS of river water samples varied from 73.8 to $230.2 \text{ mg} \cdot \text{L}^{-1}$, with an average
279 of $157.3 \text{ mg} \cdot \text{L}^{-1}$, which was comparable with the global average of $100 \text{ mg} \cdot \text{L}^{-1}$ (Gaillardet et al.,
280 1999). Compared with the major rivers in China, the average TDS was significantly lower than the
281 Changjiang (Chen et al., 2002), the Huanghe (He Jiangyi, 2017) the Zhujiang (Zhang et al., 2007),
282 the Huaihe (Zhang et al., 2011) and the Liaohe (Ding et al., 2017). However, the average TDS was
283 higher than the rivers draining silicate-rock-dominated areas, e.g., Dojiang River ($59.9 \text{ mg} \cdot \text{L}^{-1}$) in
284 Southern China (Xie Chenji, 2013), North Han River ($75.5 \text{ mg} \cdot \text{L}^{-1}$) in South Korea, (Ryu et al.,
285 2008), the Amazon ($41 \text{ mg} \cdot \text{L}^{-1}$) and the Orinoco ($82 \text{ mg} \cdot \text{L}^{-1}$) draining the Andes (Dosseto et al.,
286 2006; Edmond et al., 1996).

287

Table 1 The major physical-chemical parameters of river water samples at 15 hydrological station in the Beijiang River (mean \pm SD). The total dissolved solid

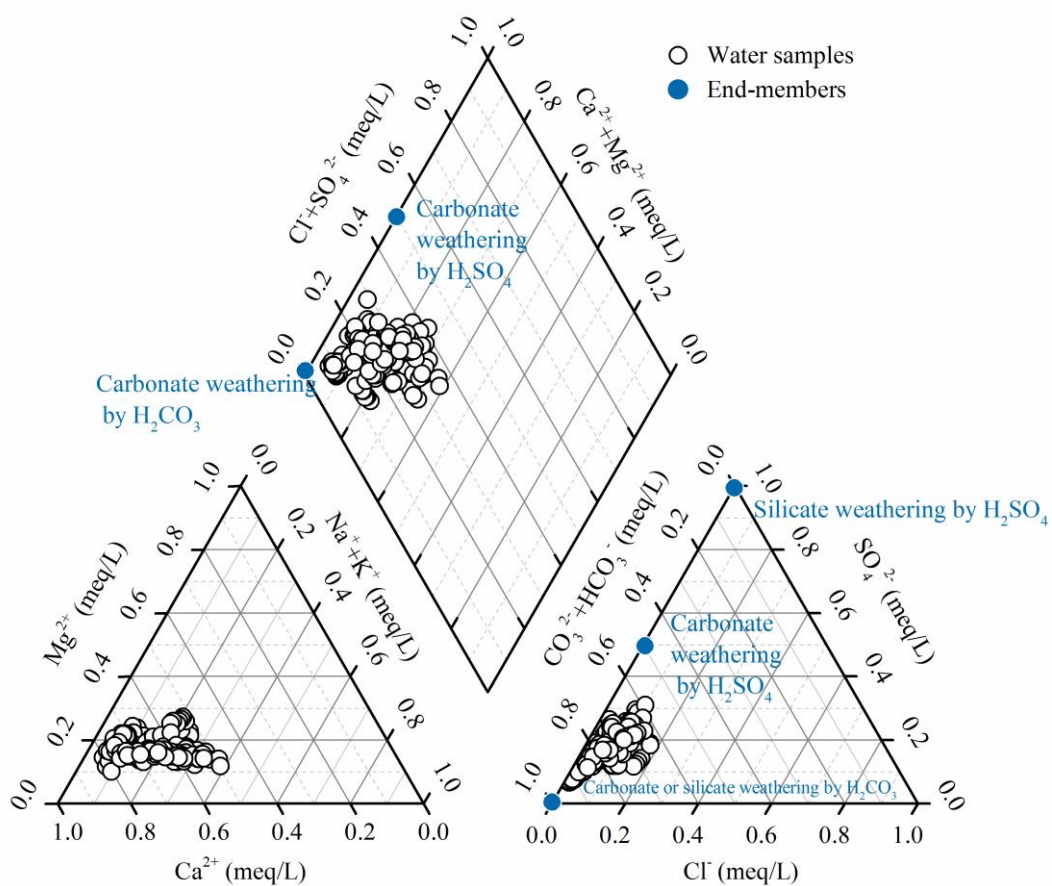
288

(TDS, mg·L⁻¹) expressed as the sum of major inorganic species concentration (Na⁺+K⁺+Ca²⁺+Mg²⁺+HCO₃⁻+Cl⁻+SO₄²⁻+NO₃⁻+SiO₂)

Hydrological stations	pH	EC (μs/cm)	TDS (mg/L)	Na ⁺ (μmol/L)	K ⁺ (μmol/L)	Ca ²⁺ (μmol/L)	Mg ²⁺ (μmol/L)	HCO ₃ ⁻ (μmol/L)	Cl ⁻ (μmol/L)	SO ₄ ²⁻ (μmol/L)	SiO ₂ (μmol/L)	HI
JLWs	7.9±0.2	95±40	81.1±25.6	111.4	51.9	223.5	103.9	701.9	28.3	44.5	225.2	0.34
CXs	8.2±0.2	219±50	163.7±20.9	118.1	40.1	793.3	187.1	1593.6	60.5	199.4	106.3	0.29
HJTs	8.1±0.2	203±34	151.8±21.9	100.2	29.9	686.7	203.9	1708.7	29.5	72.2	156.6	0.30
ZKs	8.1±0.1	218±45	161.3±21.1	426.4	66.2	560.3	134.1	1276.9	134.7	161.4	151.9	0.22
XGLs	7.8±0.2	168±16	117.9±8.9	315.4	112.4	422.4	101.0	992.2	213.9	112.6	178.9	0.18
WJs	8.1±0.1	260±27	172.9±16.7	197.8	59.0	767.3	122.6	1467.1	99.1	162.8	183.4	0.25
LXs	8.1±0.2	236±33	171.8±19.6	122.1	38.1	813.5	176.0	1829.4	51.5	89.2	145.7	0.21
LCs	8.2±0.1	253±26	196.1±20.0	287.4	46.8	862.6	234.4	1845.7	115.7	232.4	130.7	0.27
LSs	8.3±0.1	220±46	184.2±18.3	258.9	58.2	793.5	202.9	1740.6	109.0	191.9	121.4	0.25
XSs	7.9±0.1	156±30	123.9±17.6	305.0	86.1	366.8	110.9	966.6	103.8	166.5	218.7	0.24
GDs	8.1±0.1	232±11	169.4±8.3	112.6	40.5	781.6	172.1	1798.5	44.0	90.3	141.2	0.24
SKs	8.1±0.2	238±22	161.1±17.4	345.3	73.6	641.0	162.5	1304.1	174.4	223.5	160.1	0.21
Yds	7.8±0.2	241±54	165.9±34.0	296.4	59.3	674.8	160.9	1515.0	118.7	175.9	144.4	0.21
FLXs	8.0±0.2	232±37	161.4±22.8	187.6	95.1	577.0	135.0	1262.4	111.9	159.6	169.5	0.21
SJs	8.1±0.1	230±27	176.4±18.9	355.0	83.4	663.5	156.2	1367.7	182.4	190.5	180.5	0.21

289

290 Major ion compositions were shown in the Piper plot (Fig. 3). Ca^{2+} was the dominant cation
 291 with concentration ranging from 199 to 1107 $\mu\text{mol}\cdot\text{L}^{-1}$, accounting for approximately 49% to 81%,
 292 with an average of 66% (in μEq) of the total cation composition in the river water samples. HCO_3^-
 293 was the dominant anion, with concentration ranging from 640 to 2289 $\mu\text{mol}\cdot\text{L}^{-1}$. On average, it
 294 comprised 77% (59%~92%) of total anions, followed by SO_4^{2-} (16%) and Cl^- (6%). The major ionic
 295 composition indicated that the water chemistry of the Beijiang River Basin was controlled by both
 296 carbonate and silicate weathering.



297
 298 **Fig. 3 Piper plot of river water samples in the Beijiang River**

299 The PCA was used to extract the factors controlling the chemical compositions. The varimax
 300 rotation was used to reduce the number of variables to two principal components (PCs), which
 301 together explain 76.88% of the total variance in the data. The first PC (PC1) explained

302 approximately 50.02% of the total variations, and was considered to represent “carbonate
303 weathering factor” because of the high loadings of EC, TDS, Ca^{2+} , Mg^{2+} and HCO_3^- concentrations.
304 The second PC (PC2) explained 26.85% of the total variance and presented high loadings for Na^+
305 and K^+ concentrations. Thus, the PC2 represented a “silicate weathering factor”. These two PCs
306 were considered to be two important sources of major ions in the Beijiang River Basin.

307 The hydrochemical compositions of rain water were presented in Table S1. Ca^{2+} was the
308 dominant cation with concentration ranging from 6.9 to 282.6 $\mu\text{mol}\cdot\text{L}^{-1}$, accounting for
309 approximately 65% of the total cation composition in the rain water samples. SO_4^{2-} was the
310 dominant anion, with concentration ranging from 21.9 to 1462 $\mu\text{mol}\cdot\text{L}^{-1}$, accounting for
311 approximately 67% of the total anion composition in the rain water samples.

312 4.2 Seasonal and spatial variations

313 There were significant seasonal variations in the major ion concentrations (Fig. 4). Two basic
314 patterns of temporal variations could be observed. The first one was related to the carbonate
315 weathering derived ions such as Ca^{2+} and HCO_3^- , which showed high values in November and low
316 values in June. The second one was for the silicate weathering derived ions such as Na^+ and K^+ ,
317 which showed high values in February and low values in June. The minimums occurred in Jun for
318 all the ions showed a significant dilution effect during the high-flow periods.

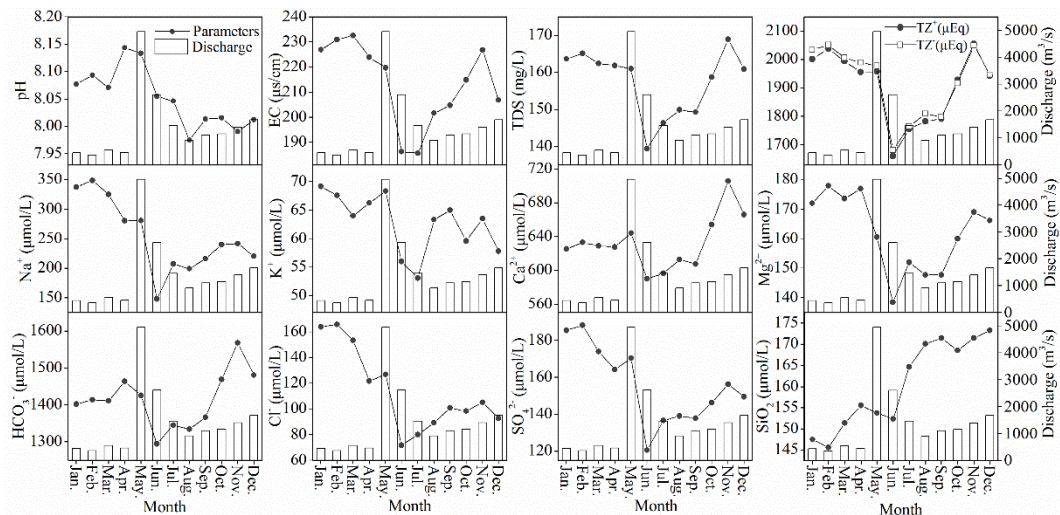


Fig. 4 Monthly variations of environmental parameters and major ion concentrations in the Beijing River Basin (SJs station). The columns denoted the monthly discharge

It was clear that the Ca^{2+} and HCO_3^- concentrations had a decreasing trend from upstream to downstream (Fig. 5), this characteristic agrees with the trends observed in the Changjiang River and the Huai River, where the major elements or TDS concentrations of the main channel showed a general decreasing trend, and the tributaries display the dilution effect to the main channel. For other silicate weathering derived ions such as Na^+ , there was a slight increasing trend implying the chemical inputs from the tributaries. These trends were in accordance with the lithology in the study area. The carbonate is dominated in the upper stream basin, when river drainages this area, carbonate weathering contributes to the elevation of Ca^{2+} and HCO_3^- . As the river entered into the downstream dominated with silicate, the relative low ion concentrations due to silicate weathering contributed to diluting the Ca^{2+} and introducing extra Na^+ to the main channel.

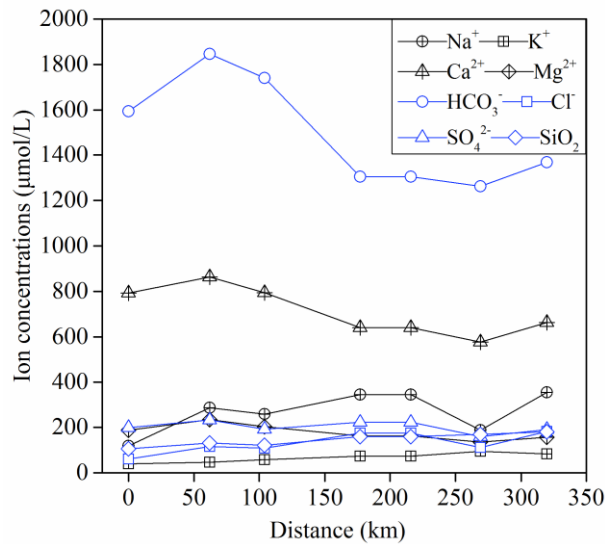


Fig. 5 Spatial variations of major ion and SiO₂ concentrations in the Beijiang River Basin (From upstream station CXs to the downstream station SJs)

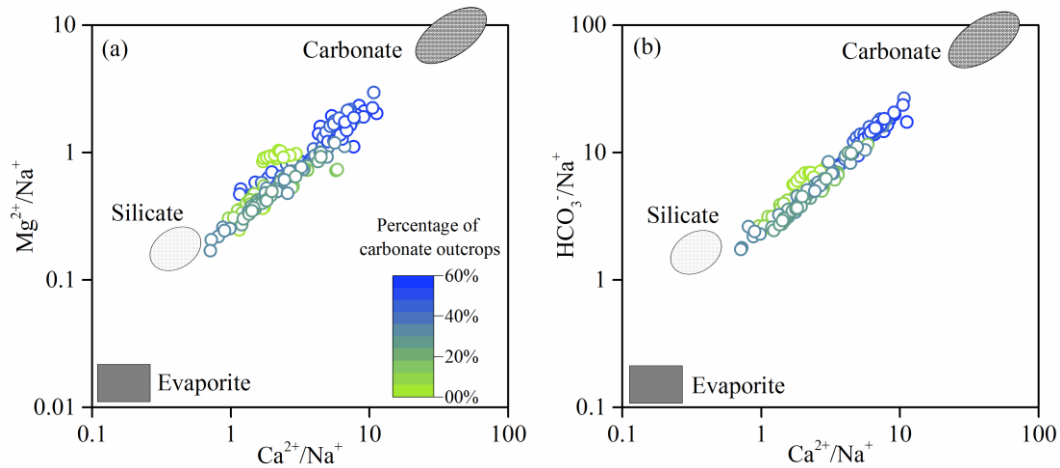
5 Discussion

5.1 Chemical weathering rates and the controlling factors

5.1.1 Chemical weathering rates

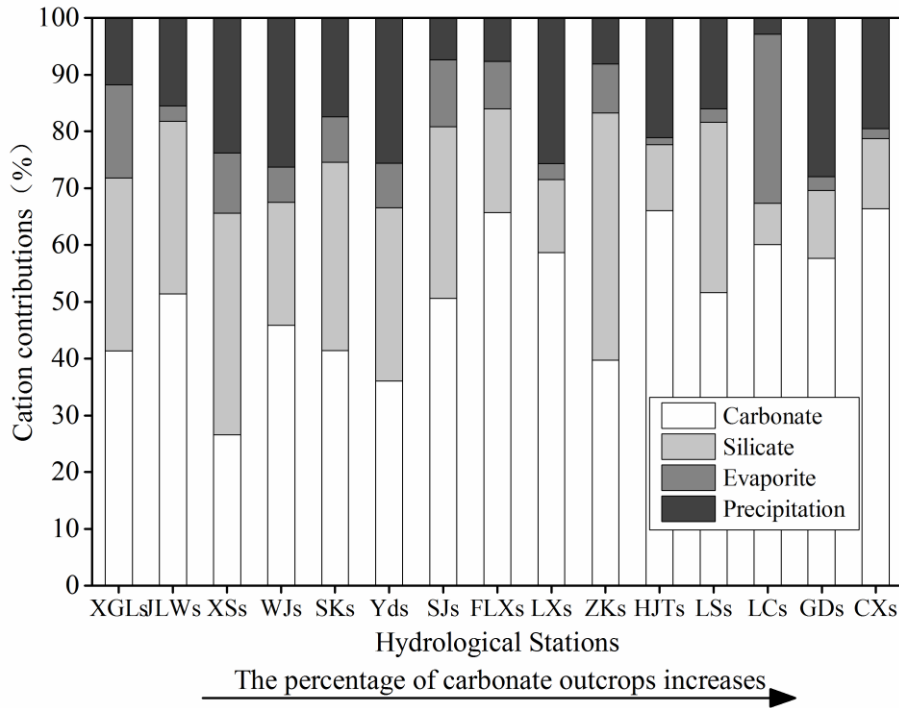
Atmospheric precipitation inputs, anthropogenic inputs (here refer to the acid deposition and AMD) and chemical weathering of rocks and minerals as the major sources contributed to the hydrochemistry in the river basin. Previous studies have shown that rock weathering contributions to major element composition of the river can be interpreted in terms of mixing among three main end-members: the weathering products of carbonates, silicates and evaporites (Cao et al., 2016b; Négrel et al., 1993; Ollivier et al., 2010). The river water samples in the Beijiang River Basin were displayed on the plots of Na-normalized molar ratios (Fig. 6). In these plots, the contributions from carbonate weathering correspond to the trend toward high-Ca²⁺ end-member close to the top right corner, while silicate weathering correspond to the trend toward to high-Na⁺ end-member close to the low-left corner. It was clear that the samples with high ratio of carbonate outcrop had the highest molar ratios of Ca²⁺/Na⁺, Mg²⁺/Na⁺ and HCO₃⁻/Na⁺, which made the samples located toward to the

349 carbonate weathering end-member. However, the samples with low $\text{Ca}^{2+}/\text{Na}^+$, $\text{Mg}^{2+}/\text{Na}^+$ and HCO_3^-
 350 $/\text{Na}^+$ ratios showed the influence of silicate weathering. In addition, major ion compositions of the
 351 Beijiang River were mainly contributed by the weathering of carbonates and silicates, and showed
 352 little contribution of evaporite weathering.



353
 354 **Fig. 6** Mixing diagrams using Na-normalized molar ratios: (a) $\text{Mg}^{2+}/\text{Na}^+$ vs. $\text{Ca}^{2+}/\text{Na}^+$ (b) HCO_3^-
 355 $/\text{Na}^+$ vs. $\text{Ca}^{2+}/\text{Na}^+$ for the Beijiang River Basin. The color ramp showed the percentage of
 356 **carbonate outcrops**

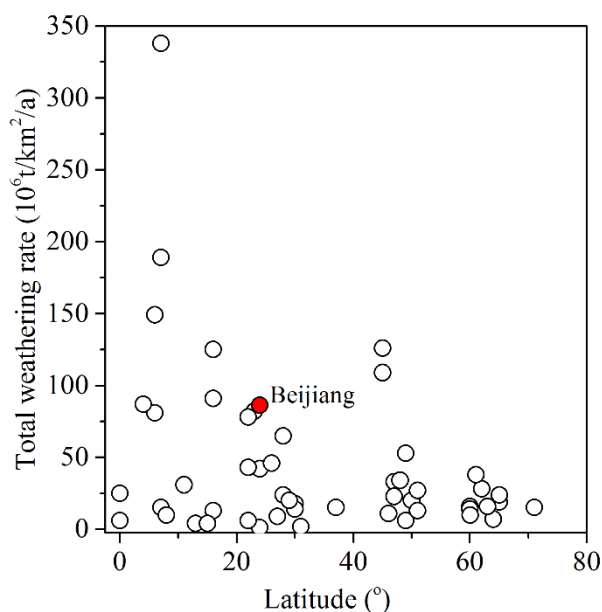
357 Based on the chemical balance method, the calculated contributions of different sources to the
 358 total cationic loads were presented in Fig. 7. The results showed that carbonate weathering was the
 359 most important mechanism controlling the local hydrochemistry, and contributed approximately
 360 50.06% (10.96%~79.96%) of the total cationic loads. Silicate weathering and atmospheric
 361 precipitation inputs accounted for 25.71% (5.55%~70.38%) and 17.92% (0~46.95%), respectively.
 362 Evaporite weathering had the minimum contribution with an average of 6.31% (0~24.36%) to the
 363 total cationic loads.



364

365 **Fig. 7** Calculate contributions (in %) from the different hydrological stations to the total cationic
 366 load in the Beijiing River Basin. The cationic loads were the sum of Na⁺, K⁺, Ca²⁺ and Mg²⁺

367 The result of chemical weathering rates was listed in Table 2. The carbonate weathering
 368 contributes about 70% of the total chemical weathering, and the average of carbonate and silicate
 369 weathering rate in the Beijiing River Basin were 61.15 and 25.31 t·km⁻²·a⁻¹, respectively. In addition,
 370 chemical weathering rates showed significantly seasonal variations with the highest carbonate and
 371 silicate weathering rates in May (16.75 and 5.50 t·km⁻²·month⁻¹, respectively) and the lowest
 372 carbonate and silicate weathering rates in February (0.95 and 0.39 t·km⁻²·month⁻¹, respectively).
 373 Gaillardet et al. (1999) reported the chemical weathering rate of major rivers all over the world and
 374 found that the hyperactive zone with high chemical weathering rate is generally located between the
 375 latitude 0-30° and our study belongs to this area (Fig. 8). The factors influence the balance between
 376 CWR and SWR would be further discussed in the following parts.



377

378

Fig. 8 Relationship between latitude and total weathering rate (TWR)

379

Table 2 The annual discharge, catchment area, carbonate and silicate outcrops proportions, and

380

calculated weathering rates of carbonate and silicate of 15 subcatchments in the Beijiang River

ID	Annual discharge (10 ⁸ m ³ /a)	Catchment area (km ²)	Percentages of carbonate (%)	Percentages of silicate (%)	Carbonate weathering rate -CWR (t km ⁻² year ⁻¹)	Silicate weathering rate -SWR (t km ⁻² year ⁻¹)	Total weathering rate -TWR (t km ⁻² year ⁻¹)
JLWs	2.23	281.13	2.95	97.05	18.63	14.94	33.56
CXs	4.06	392.35	57.44	42.56	74.21	11.42	85.64
HJTs	11.54	503.02	41.99	55.83	169.12	29.73	198.85
ZKs	16.38	1655.22	34.60	61.81	35.03	24.14	59.17
XGLs	13.56	1863.02	0.38	93.07	25.75	13.96	39.72
WJs	19.11	1960.99	12.51	73.87	55.00	17.43	72.43
LXs	56.37	2458.06	34.32	64.07	178.71	29.39	208.10
LCs	58.74	5278.14	49.67	50.21	79.70	20.59	100.29
LSs	74.83	6994.69	44.59	52.44	69.28	14.94	84.22
XSs	62.11	7497.01	7.09	87.81	18.85	20.35	39.20
GDs	137.81	9028.38	49.93	44.93	111.73	19.19	130.92
SKs	49.51	17417.24	25.43	69.35	12.71	6.11	18.82
YDs	191.07	18234.64	25.63	68.05	52.37	19.59	71.95
FLXs	396.25	34232.34	29.68	63.49	68.38	17.53	85.91
SJs(Average)	450.90	38538.06	28.12	64.65	61.15	25.31	86.46

381

5.1.2 Factors affecting chemical weathering

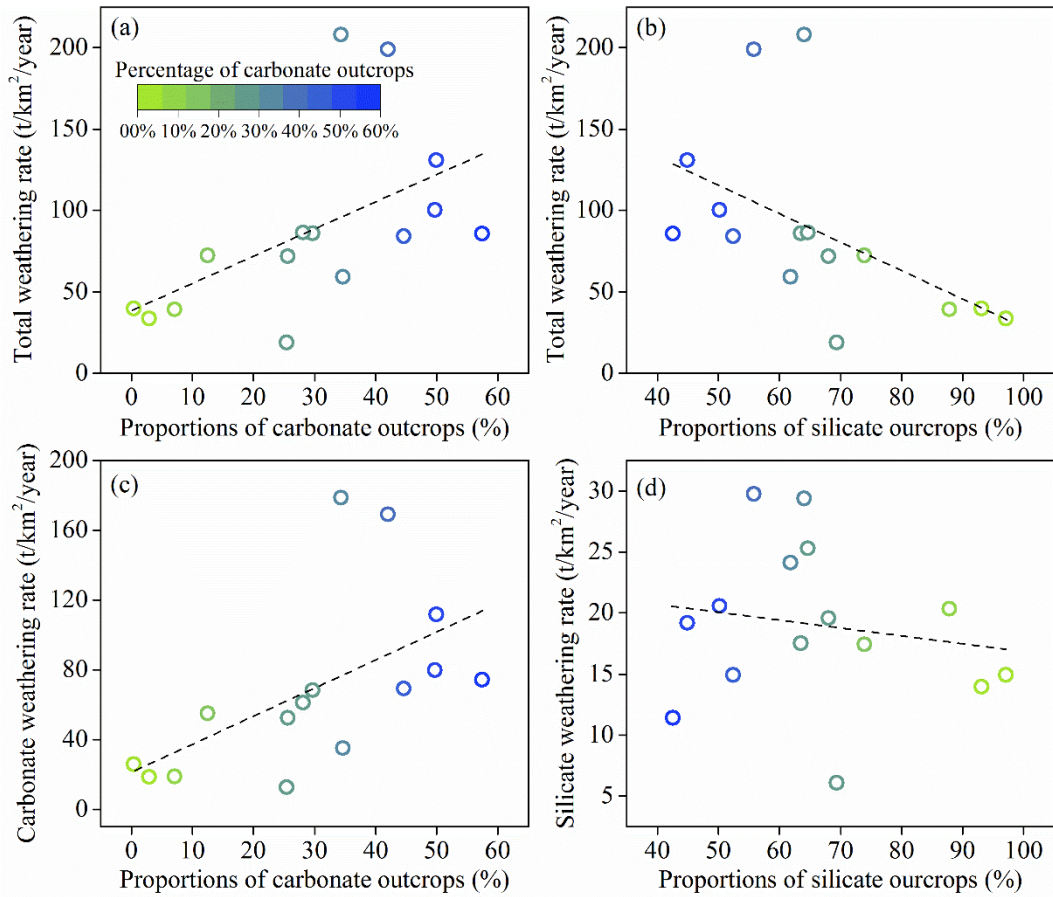
382

Many factors control the chemical weathering rates, including terrain, geotectonic properties,

383 lithology, land cover, climatic conditions (temperature, precipitation, etc.), and hydrological
384 characteristics (Ding et al., 2017; Gislason et al., 2009; Hagedorn and Cartwright, 2009). For this
385 study, the lithology, hydrological characteristics and geomorphology was selected as the major
386 factors to be discussed.

387 **5.1.2.1 Lithology**

388 Among all the factors controlling the chemical weathering rates, lithology is one of the most
389 important factors because different type of rocks has different weathering abilities (Viers et al.,
390 2014). The TWR had a significant positive correlation ($p < 0.01$) with the ratios of the proportion of
391 carbonate and a non-significant positive correlation with that of silicate outcrops (Fig. 9a, b).
392 Furthermore, a significant correlation ($p < 0.01$) was found between the CWR and proportion of
393 carbonate outcrops (Fig. 9c), but the correlation between the SWR and the proportion of silicate
394 outcrops was low and not statistically significant ($p > 0.05$, Fig. 9d). The correlation analysis
395 confirmed that carbonate outcrops ratios was the sensitive factor controlling the chemical
396 weathering rates and the rapid kinetics of carbonate dissolution played an important role in
397 weathering rates in the Beijiang River Basin.



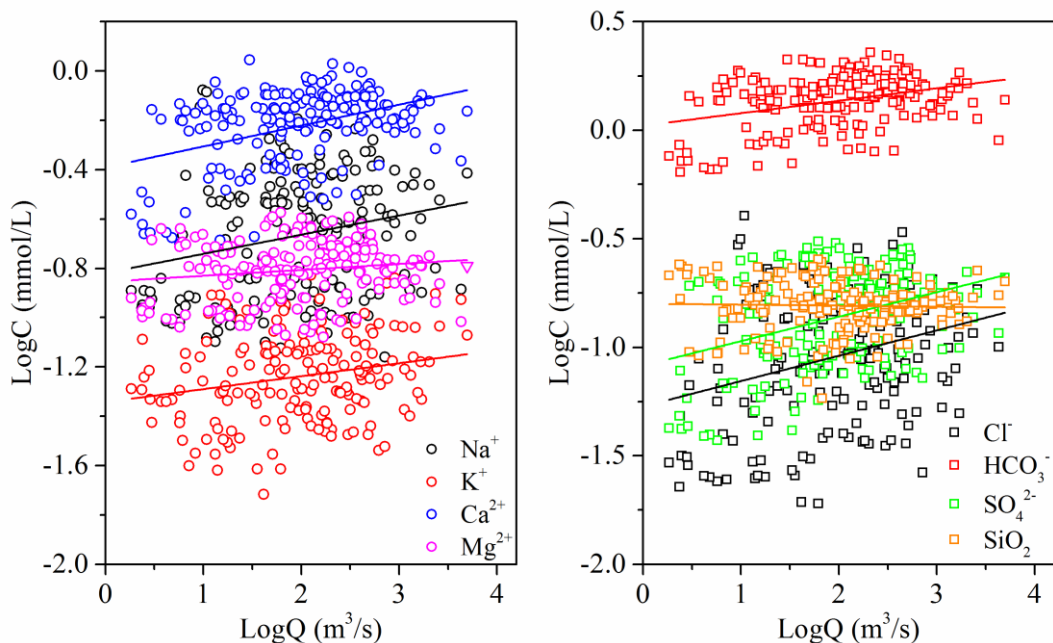
398
 399 **Fig. 9** The relationships between weathering rates and the proportions of carbonate or silicate
 400 **outcrops**

401 **5.1.2.2 Runoff**

402 Chemical weathering is a combination of two processes, including dissolution of primary
 403 minerals and precipitation of secondary minerals growth (Eiriksdottir et al., 2011; Hartmann et al.,
 404 2014a; Liu et al., 2013). The dissolution process is quite related to the precipitation and runoff. In
 405 general, river water chemistry is usually diluted by river runoff (Q), and this dilution effect is
 406 variable in different basins (Rao et al., 2019). The dilution effects of major element caused by
 407 increasing water flow can be expressed by log linear equation, the standard rating relationship (Li
 408 et al., 2014; Walling, 1986; Zhang et al., 2007):

409
$$C_i = aQ^b \quad (34)$$

410 where C_i is the concentration of element i (mmol/L), Q is the water discharge (m^3/s), a is the
 411 regression constant and b is the regression exponent. The linear fitting result was showed by Fig. 10
 412 and the parameters b for major elements obtained from the dataset were 0.08 (Na^+), 0.05 (K^+), 0.08
 413 (Ca^{2+}), 0.02 (Mg^{2+}), 0.06 (HCO_3^-), 0.12 (Cl^-), 0.11 (SO_4^{2-}) and -0.005 (SiO_2), respectively. In many
 414 cases, b ranges from -1 to 0 due to the chemical variables that are influenced in various ways and
 415 various extents. However, in our study area, the values of b were positive and not comparable to the
 416 observations in the major Asian River such as the Yangtze (Chen et al., 2002), the Yellow (Chen et
 417 al., 2005), the Pearl Rivers (Zhang et al., 2007) and the Mekong River (Li et al., 2014). This
 418 suggested additional and significant solute sources in the river basin that might contribute and
 419 compensate considerably the effect of dilution by precipitation. The difference of slope for
 420 individual dissolved components at different stations reflected the different sources and the
 421 solubility of source materials.



422
 423 **Fig. 10** The relationship between major ion concentrations and runoff (Q) in logarithmic scales

424 Due to the compensation effect of chemical weathering, significant positive linear relationship

425 was detected between Q and TWR, CWR and SWR. So that, the linear regression analysis between
 426 Q and TWR, CWR and SWR were conducted to further reveal the effect of runoff on chemical
 427 weathering rate. The slope of the liner regression equations for all 15 hydrological station
 428 watersheds in the Beijiing River Basin were summarized in Table 3. The linear relations indicated
 429 that the increase of runoff could accelerate the chemical weathering rates, but the variations of K
 430 values revealed that the degrees of influences were different due to multiple factor influence, such
 431 as the influence of geomorphology.

432 **Table 3 The slope of the liner regression equation between runoff (Q) and total weathering rate**
 433 **(TWR), carbonate weathering rate (CWR) and silicate weathering rate (SWR)**

Hydrological stations	Total weathering rate =K ₁ Q		Carbonate weathering rate =K ₂ Q		Silicate weathering rate =K ₃ Q	
	K ₁	R ²	K ₂	R ²	K ₃	R ²
JLWs	0.3912	0.99	0.2091	0.99	0.1821	0.99
CXs	0.6492	0.93	0.5631	0.93	0.0860	0.94
HJTs	0.5117	0.97	0.4421	0.96	0.0695	0.99
ZKs	0.0953	0.97	0.0525	0.76	0.0429	0.80
XGLs	0.0835	0.98	0.0558	0.97	0.0278	0.98
WJs	0.1017	0.99	0.0842	0.99	0.0175	0.88
LXs	0.0968	0.98	0.0843	0.98	0.0125	0.99
LCs	0.0486	0.90	0.0401	0.87	0.0085	0.97
LSs	0.0359	0.97	0.0286	0.96	0.0073	0.94
XSs	0.0180	0.98	0.0080	0.97	0.0100	0.96
GDs	0.0252	0.99	0.0216	0.99	0.0036	0.99
SKs	0.0116	0.98	0.0083	0.98	0.0033	0.95
Yds	0.0106	0.99	0.0081	0.99	0.0026	0.92
FLXs	0.0050	0.97	0.0039	0.95	0.0010	0.99
SJs	0.0053	0.99	0.0037	0.97	0.0016	0.98

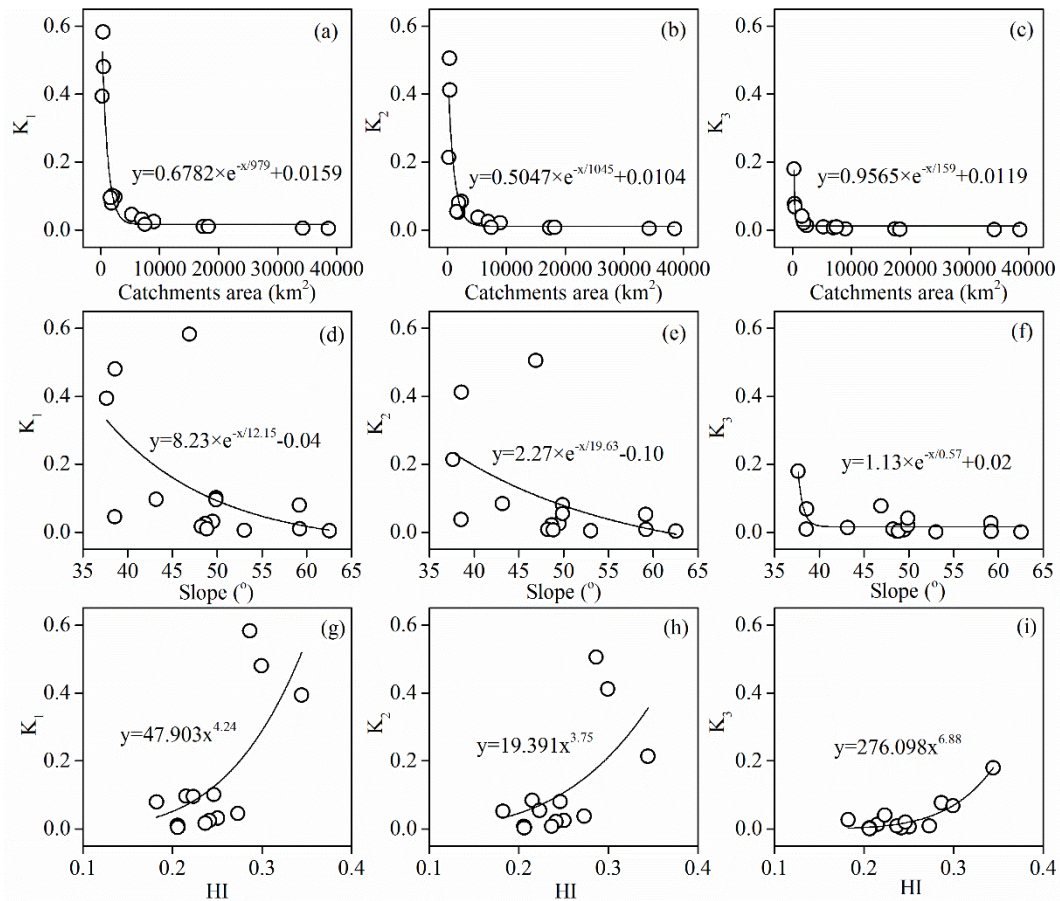
434 5.1.2.3 Geomorphology

435 The geomorphology factors including catchment area, average slope and HI, which could quite

436 influence the runoff generation process and physical and chemical weathering, were selected to give
437 a further explanation of the variation of K values. As showed in Fig. 11a, the K values were found
438 a non-linear relationship with the areas of subcatchment and could be fitted by exponential decay
439 model, which showed that the K values decreased dramatically with the initial increasing of area
440 and quickly become stable after reaching the threshold. The threshold value for K_1 , K_2 and K_3 was
441 about 5000 km². It indicated that the compensation effect was more significant in small catchment.

442 The average topographic slope of each subcatchment ranged from 37° to 63°. With the
443 increasing of average slope, the residence time of both surface water and groundwater decrease.
444 Kinetics of carbonate and silicate reactions was determined by the reaction time which could be
445 related by the residence time of water. In our study area, the K values showed non-linear negative
446 correlation with average slope (Fig. 11e, f, g). When the average slope increase, the resulted small
447 residence time (time of water-rock reactions) make the compensation effect also weak in the study
448 area.

449 Hypsometric analysis showed that the HI ranged from 0.18 to 0.34. According to the empirical
450 classification by HI ($HI > 0.6$, inequilibrium or young stage, $0.35 < HI \leq 0.6$, equilibrium or mature
451 stage, $HI \leq 0.35$, monadnock or old age), the geomorphological development in the Beijiang River
452 was recognized as the old age, which reflect the erodible degree and erosion trend of the
453 geomorphology was high. Furthermore, the non-linear positive correlations between HI and K
454 values (Fig. 11g, h, i) also addressed that geomorphology development have significant influence
455 on chemical weathering and relating CO₂ consumption processes.



456

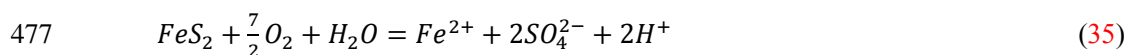
457 **Fig. 11** The relationships between K values and catchments area (a, b, c), average slope (d, e, f)
 458 and HI (g, h, i) for the Beijiang River.

459 **5.2 Temporary and net sink of atmospheric CO₂**

460 **5.2.1 Sulfate origin and DIC apportionment**

461 The successful application of DIC apportionment calculation mentioned in section 3.2.2 is
 462 depended on the origins of sulfate (SO₄²⁻). Three origins of SO₄²⁻ should be discriminated
 463 including atmospheric acid deposition (Larssen and Carmichael, 2000), acid mining discharge
 464 (AMD) (Li et al., 2018; Li et al., 2019) and chemical weathering of evaporite such as the dissolution
 465 of gypsum (Appelo and Postma, 2005). Acid rain events occurred frequently in South and East
 466 China after 1980 (Larssen et al., 2006). The pH isolines based on data from 86 monitoring stations
 467 (Larssen et al., 2006) showed that in the Beijiang River the rain pH was lower than 4.5 and our
 468 monitoring dataset also proved this result. Sulfur wet deposition estimated based on the observed

469 bulk wet sulfur deposition data and the RAINS-Asia model (Larssen and Carmichael, 2000) ranged
470 from 2000-5000 eq ha⁻¹ a⁻¹, which showed that the acid sulfur deposition was one of the most
471 important sources of river sulfate. In addition, considering the abundant ore resources in the Beijiang
472 River, the second possible source of SO₄²⁻ is sulfide oxidation due to mining. In our previous study,
473 the SO₄²⁻ with AMD origin mainly came from the tributary Wenjiang River (Wen et al., 2018). These
474 two sources could offer sufficient chemical weathering agent H₂SO₄ and actively involved in the
475 chemical weathering due to the following reaction mechanism (take carbonate for example) (Taylor
476 et al., 1984; van Everdingen and Krouse, 1985).



479 The third source came from dissolution of gypsum could not offer active H₂SO₄ to induce
480 carbonate and silicate dissolution. Two evidences were summarized to indicate the absence of
481 gypsum in the study area, (1) Lithology in the river basin is composed of limestone, sandstone,
482 gneiss and glutenite. HI showed that geomorphology development has entered into the “old” age,
483 the evaporite such as halite and gypsum has been consumed by the dissolution. (2) The
484 stoichiometric relationship between Ca²⁺ and SO₄²⁻ (错误!未找到引用源。) showed that all of the
485 samples in the study area located below the 1:1 gypsum dissolution line, and they also below the
486 1:2 carbonate weathering induced by sulfuric acid (SCW) line. These two points combined gave the
487 evidence to prove the absence of contribution of gypsum dissolution to river SO₄²⁻. So that, the DIC
488 apportionment could be calculated according to equation (18) to (21) and the result of three main
489 processes (CCW, CSW and SCW) contributing to the DIC origin in the Beijiang River water are
490 showed in Table 4. It was found that CCW was the dominant origin of DIC (35%~87%) and that

491 SCW (3%~15%) and CSW (7%~59%) were non-negligible weathering processes.

492 **5.2.2 Temporary and net CO₂ sink**

493 According to the classical view of the global carbon cycling (Berner and Kothavala, 2001),
494 the CO₂ sink induced by chemical weathering varies for different time scales. At short-term
495 timescale, carbonic acid based carbonate and silicate weathering (CCW and CSW) and transport of
496 the HCO₃⁻ to oceans through rivers is an important “temporary” carbon sink (Khadka et al., 2014)
497 and can be calculated by the sum of CCR_{CCW} and CCR_{CSW}. Thus, it was significant to estimate the
498 CCR of CCW and CSW (Liu and Dreybrodt, 2015; Liu et al., 2011). However, at the geological
499 timescale (>10⁶ years), when over the timescale typical of residence time of HCO₃⁻ in the ocean
500 (10⁵ years), the CCW is not a mechanism that can participate in the net sink of CO₂ in the atmosphere
501 because all of the atmospheric CO₂ fixed through CCW is returned to the atmosphere during
502 carbonate precipitation in the ocean. Meanwhile, in case of CSW, followed by carbonate deposition,
503 one of the two moles of CO₂ involved is transferred from the atmosphere to the lithosphere in the
504 form of carbonate rocks, while the other one returns to the atmosphere. The CSW is recognized as
505 the net sink of atmosphere CO₂. In addition, when sulfuric acid is involved as a proton donor in
506 carbonate weathering, half of the carbon dissolved to the atmospheric during carbonate precipitation.
507 Thus, SCW leads to a net release of CO₂ in ocean-atmosphere system. So that the net CO₂ sink
508 (expressed by CCR_{Net} in this study) is controlled by the DIC apportionment according to equation
509 (31).

510 The results of CCR_{Total}, CCR_{CCW}, CCR_{CSW} and CCR_{Net} were summarized in Table 4. The
511 CCR_{Total} was 823.41 10³ mol km⁻² a⁻¹. Comparing with other Chinese rivers, such as the Songhua
512 River (189×10³ mol km⁻² a⁻¹) (Cao et al., 2015) and other rivers calculated by (Gaillardet et al.,

1999) including the Heilong River ($53 \times 10^3 \text{ mol km}^{-2} \text{ a}^{-1}$), the Changjiang River ($609 \times 10^3 \text{ mol km}^{-2} \text{ a}^{-1}$), the Huanghe River ($360 \times 10^3 \text{ mol km}^{-2} \text{ a}^{-1}$), the Xijiang River ($960 \times 10^3 \text{ mol km}^{-2} \text{ a}^{-1}$), the Jinshajiang River ($420 \times 10^3 \text{ mol km}^{-2} \text{ a}^{-1}$), the Lancangjiang River ($980 \times 10^3 \text{ mol km}^{-2} \text{ a}^{-1}$), the Nujiang River ($1240 \times 10^3 \text{ mol km}^{-2} \text{ a}^{-1}$), the Yalongjiang River ($870 \times 10^3 \text{ mol km}^{-2} \text{ a}^{-1}$), the Daduhe River ($1280 \times 10^3 \text{ mol km}^{-2} \text{ a}^{-1}$) and Minjiang River ($660 \times 10^3 \text{ mol km}^{-2} \text{ a}^{-1}$), our study area showed relative high CCR due to high chemical weathering rate. In addition, the CCR_{CCW} and CCR_{CSW} were 536.59×10^3 (65%) and 286.82×10^3 (35%) $\text{mol km}^{-2} \text{ a}^{-1}$, respectively. Compared with the “temporary” sink, the net sink of CO_2 for the Beijiang River was approximately $23.18 \times 10^3 \text{ mol km}^{-2} \text{ a}^{-1}$ of CO_2 sinking in the perspective of global carbon cycling. It was about 3% of the “temporary” CO_2 sink. In addition, the CO_2 net sink of each sub basin were also different and show large spatial variations due to heterogeneity of geology and human activities. The geology showed weak correlation with the CO_2 net sink (Fig. 12a), while the $[\text{SO}_4^{2-}]_{SCW}$ and $[\text{SO}_4^{2-}]_{SSW}$ have weak negative correlation with the CO_2 net sink (Fig. 12b). It proved that human activities (sulfur acid deposition and AMD) decreased the CO_2 net sink and even make chemical weathering a CO_2 source to the atmosphere.

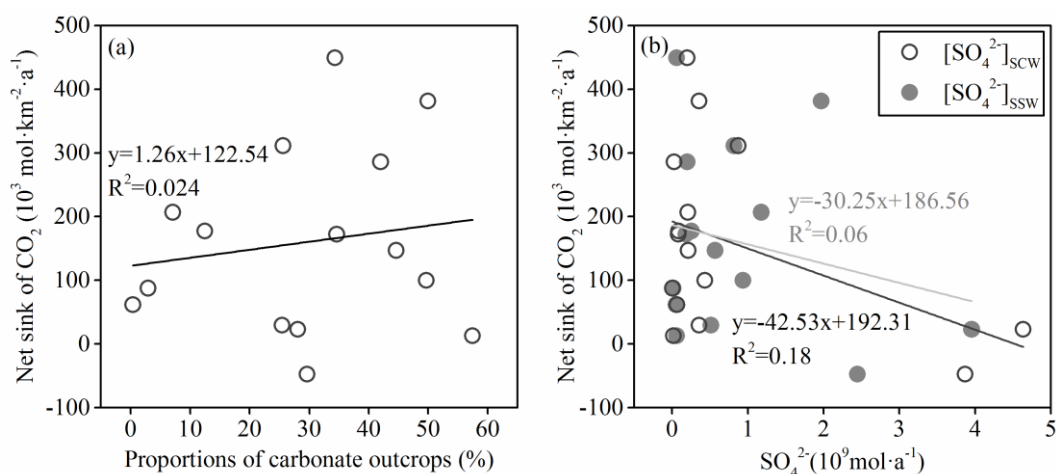
Table 4 Calculated CO_2 consumption rate and net sink of 15 nested subcatchments in the

Beijiang River Basin

Hydrological stations	DIC apportionment (10^9 mol a^{-1})			“Temporary” Sink (CO_2 consumption rate) ($10^3 \text{ mol km}^{-2} \text{ a}^{-1}$)			Net Sink ($10^3 \text{ mol km}^{-2} \text{ a}^{-1}$)
	CCW	SCW	CSW	CCR_{CCW}	CCR_{CSW}	CCR_{Total}	CCR_{Net}
JLWs	0.10	0.00	0.05	175.23	191.14	366.36	87.73
CXs	0.57	0.04	0.05	732.05	118.18	850.23	13.18
HJTs	1.57	0.06	0.34	1563.64	683.41	2247.05	286.14
ZKs	1.24	0.16	0.73	375.23	439.77	815.00	172.27
XGLs	0.85	0.14	0.37	227.05	195.91	422.95	61.59

WJs	1.76	0.17	0.87	449.32	443.18	892.50	177.50
LXs	7.30	0.40	2.61	1485.45	1060.45	2545.91	449.09
LCs	8.07	0.86	1.92	764.32	363.41	1127.95	99.77
LSs	10.13	0.42	2.48	724.55	354.32	1078.64	147.05
XSs	2.08	0.41	3.52	138.64	469.09	607.73	207.05
GDs	16.48	0.71	7.60	912.73	841.82	1754.55	381.36
SKs	4.00	0.72	1.74	114.77	100.23	215.00	29.55
YDs	14.11	1.75	13.10	386.82	718.64	1105.45	311.14
FLXs	40.38	7.74	4.46	589.77	130.45	720.23	-47.73
SJs	41.36	9.27	11.05	536.59	286.82	823.41	23.18

530



531

532 **Fig. 12 Correlations between CO₂ net sinks and proportions of carbonate (a) and**
 533 **correlations between CO₂ net sinks and [SO₄²⁻]_{scw} or [SO₄²⁻]_{ssw} (b)**

534 6 Conclusions

535 This study revealed the temporary and net sinks of atmospheric CO₂ due to chemical
 536 weathering in a subtropical hyperactive catchment with mixing carbonate and silicate lithology
 537 under the stress of chemical weathering induced by anthropogenic sulfuric acid agent. During the
 538 sampling period, the pH values ranged from 7.5 to 8.5 and TDS varied from 73.8 to 230.2 mg·L⁻¹.
 539 Ca²⁺ and HCO₃⁻ were the dominated cation and anion. Water chemical patterns and PCA showed
 540 that carbonate and silicate weathering were the most important processes controlling the local

541 hydrochemistry. In average, carbonate and silicate weathering contributed approximately 50.06%
542 and 25.71% of the total cationic loads, respectively.

543 The average of carbonate and silicate weathering rate in the Beijiang River Basin were 61.15
544 and 25.31 $\text{t}\cdot\text{km}^{-2}\cdot\text{a}^{-1}$, respectively. The high rate was comparable to other rivers located in the
545 hyperactive zone between the latitude 0-30°. The lithology, runoff and geomorphology had
546 significant influences on the chemical weathering rate. (1) Due to the difference between kinetics
547 of carbonate and silicate dissolution processes, the proportion of carbonate outcrops had significant
548 positive correlation with the chemical weathering rate and confirmed that carbonate outcrops ratios
549 was the sensitive factor controlling the chemical weathering rates and the rapid kinetics of carbonate
550 dissolution played an important role in weathering rates. (2) Runoff mainly controlled the season
551 variations and the dilution effect was weak in the study area. Due to the compensation effect of
552 chemical weathering, significant positive linear relationship was detected between Q and TWR,
553 CWR and SWR. (3) The geomorphology factors such as slope and HI had non-linear correlation on
554 chemical weathering rate and showed significant scale effect, which revealed the complexity in
555 chemical weathering processes.

556 DIC apportionment showed that CCW was the dominant origin of DIC (35%-87%) and that
557 SCW (3%-15%) and CSW (7%-59%) were non-negligible weathering processes. The $\text{CCR}_{\text{Total}}$ was
558 $823.41 \times 10^3 \text{ mol km}^{-2} \text{ a}^{-1}$, relative high CCR due to high chemical weathering rate. In addition, the
559 CCR_{CCW} and CCR_{CSW} were 536.59×10^3 (65%) and 286.82×10^3 (35%) $\text{mol km}^{-2} \text{ a}^{-1}$, respectively.
560 Compared with the “temporary” sink, the net sink of CO_2 for the Beijiang River was approximately
561 $23.18 \times 10^3 \text{ mol km}^{-2} \text{ a}^{-1}$ of CO_2 sinking in the perspective of global carbon cycling. It was about
562 2.82% of the “temporary” CO_2 sink. Human activities such as sulfur acid deposition and AMD have

563 significantly altered the CO₂ sinks.

564 **7 Acknowledgments**

565 This research work was financially supported by the General Program of the National Natural
566 Science Foundation of China (No.41877470), the Natural Science Foundation of Guangdong
567 Province, China (No. 2017A030313231) and the Natural Science Foundation of Guangdong
568 Province, China (No. 2017A030313229).

569 **8 Code/Data availability:** Yes.

570 **9 Author contribution:** Cao Yingjie and Tang Changyuan designed the study, carried out the
571 field work, analyzed the results, and drafted the manuscript. Xuan Yingxue and Guan Shuai
572 participated in the field sampling and laboratory analysis. Peng Yisheng reviewed and edited the
573 original draft of the manuscript. All authors read and approved the final manuscript.

574 **10 Competing interests:** No.

575 **References**

- 576 Appelo, C. A. J., and Postma, D.: *Geochemistry, groundwater and pollution*, CRC press, 2005.
- 577 Berner, R. A., and Kothavala, Z.: GEOCARB III: a revised model of atmospheric CO₂ over
578 Phanerozoic time, *American Journal of Science*, 301, 182-204, 0002-9599, 2001.
- 579 Cao, Y., Tang, C., Song, X., and Liu, C.: Major ion chemistry, chemical weathering and CO₂
580 consumption in the Songhua River basin, Northeast China, *Environmental Earth Sciences*, 73,
581 7505-7516, 2015.
- 582 Cao, Y., Tang, C., Cao, G., and Wang, X.: Hydrochemical zoning: natural and anthropogenic origins
583 of the major elements in the surface water of Taizi River Basin, Northeast China,
584 *Environmental Earth Sciences*, 75, 1-14, 2016b.
- 585 Chen, J., Wang, F., Xia, X., and Zhang, L.: Major element chemistry of the Changjiang (Yangtze
586 River), *Chemical Geology*, 187, 231-255, 2002.
- 587 Chen, J., Wang, F., Meybeck, M., He, D., Xia, X., and Zhang, L.: Spatial and temporal analysis of
588 water chemistry records (1958–2000) in the Huanghe (Yellow River) basin, *Global*
589 *biogeochemical cycles*, 19, 2005.
- 590 Ding, H., Liu, C.-Q., Zhao, Z.-Q., Li, S.-L., Lang, Y.-C., Li, X.-D., Hu, J., and Liu, B.-J.:
591 Geochemistry of the dissolved loads of the Liao River basin in northeast China under
592 anthropogenic pressure: Chemical weathering and controlling factors, *Journal of Asian Earth*
593 *Sciences*, 138, 657-671, <https://doi.org/10.1016/j.jseaes.2016.07.026>, 2017.
- 594 Donnini, M., Frondini, F., Probst, J.-L., Probst, A., Cardellini, C., Marchesini, I., and Guzzetti, F.:
595 Chemical weathering and consumption of atmospheric carbon dioxide in the Alpine region,

596 Global and Planetary Change, 136, 65-81, <https://doi.org/10.1016/j.gloplacha.2015.10.017>,
597 2016.

598 Dosseto, A., Bourdon, B., Gaillardet, J., Allègre, C. J., and Filizola, N.: Time scale and conditions
599 of weathering under tropical climate: Study of the Amazon basin with U-series, *Geochimica et*
600 *Cosmochimica Acta*, 70, 71-89, <https://doi.org/10.1016/j.gca.2005.06.033>, 2006.

601 Edmond, J. M., Palmer, M. R., Measures, C. I., Brown, E. T., and Huh, Y.: Fluvial geochemistry of
602 the eastern slope of the northeastern Andes and its foredeep in the drainage of the Orinoco in
603 Colombia and Venezuela, *Geochimica et Cosmochimica Acta*, 60, 2949-2974,
604 [https://doi.org/10.1016/0016-7037\(96\)00142-1](https://doi.org/10.1016/0016-7037(96)00142-1), 1996.

605 Eiriksdottir, E. S., Gislason, S. R., and Oelkers, E. H.: Does runoff or temperature control chemical
606 weathering rates?, *Applied Geochemistry*, 26, S346-S349,
607 <https://doi.org/10.1016/j.apgeochem.2011.03.056>, 2011.

608 Fernandes, A. M., Conceição, F. T. d., Spatti Junior, E. P., Sardinha, D. d. S., and Mortatti, J.:
609 Chemical weathering rates and atmospheric/soil CO₂ consumption of igneous and
610 metamorphic rocks under tropical climate in southeastern Brazil, *Chemical Geology*, 443, 54-
611 66, <https://doi.org/10.1016/j.chemgeo.2016.09.008>, 2016.

612 Gaillardet, J., Dupré, B., Louvat, P., and Allègre, C. J.: Global silicate weathering and CO₂
613 consumption rates deduced from the chemistry of large rivers, *Chemical Geology*, 159, 3-30,
614 [https://doi.org/10.1016/S0009-2541\(99\)00031-5](https://doi.org/10.1016/S0009-2541(99)00031-5), 1999.

615 Galy, A., and France-Lanord, C.: Weathering processes in the Ganges–Brahmaputra basin and the
616 riverine alkalinity budget, *Chemical Geology*, 159, 31-60, [https://doi.org/10.1016/S0009-2541\(99\)00033-9](https://doi.org/10.1016/S0009-2541(99)00033-9), 1999.

617

618 Gao, Q., Tao, Z., Huang, X., Nan, L., Yu, K., and Wang, Z.: Chemical weathering and CO₂
619 consumption in the Xijiang River basin, South China, *Geomorphology*, 106, 324-332,
620 <https://doi.org/10.1016/j.geomorph.2008.11.010>, 2009.

621 Garrels, R. M.: The carbonate-silicate geochemical cycle and its effect on atmospheric carbon
622 dioxide over the past 100 million years, *Am J Sci*, 283, 641-683, 1983.

623 Gibbs, R. J.: Water chemistry of the Amazon River, *Geochimica et Cosmochimica Acta*, 36, 1061-
624 1066, [https://doi.org/10.1016/0016-7037\(72\)90021-X](https://doi.org/10.1016/0016-7037(72)90021-X), 1972.

625 Gislason, S. R., Oelkers, E. H., Eiriksdottir, E. S., Kardjilov, M. I., Gisladottir, G., Sigfusson, B.,
626 Snorrason, A., Elefsen, S., Hardardottir, J., Torssander, P., and Oskarsson, N.: Direct evidence
627 of the feedback between climate and weathering, *Earth and Planetary Science Letters*, 277,
628 213-222, <https://doi.org/10.1016/j.epsl.2008.10.018>, 2009.

629 Guo, J., Wang, F., Vogt, R. D., Zhang, Y., and Liu, C. Q.: Anthropogenically enhanced chemical
630 weathering and carbon evasion in the Yangtze Basin, *Scientific Reports*, 5, 11941, 2015.

631 Hagedorn, B., and Cartwright, I.: Climatic and lithologic controls on the temporal and spatial
632 variability of CO₂ consumption via chemical weathering: An example from the Australian
633 Victorian Alps, *Chemical Geology*, 260, 234-253,
634 <https://doi.org/10.1016/j.chemgeo.2008.12.019>, 2009.

635 Hartmann, J., Jansen, N., Dürr, H. H., Kempe, S., and Köhler, P.: Global CO₂-consumption by
636 chemical weathering: What is the contribution of highly active weathering regions?, *Global*
637 *and Planetary Change*, 69, 185-194, <https://doi.org/10.1016/j.gloplacha.2009.07.007>, 2009.

638 Hartmann, J., Moosdorf, N., Lauerwald, R., Hinderer, M., and West, A. J.: Global chemical
639 weathering and associated P-release - The role of lithology, temperature and soil properties,

640 Chemical Geology, 363, 145-163, <https://doi.org/10.1016/j.chemgeo.2013.10.025>, 2014a.

641 Hartmann, J., West, J., Renforth, P., Köhler, P., Rocha, C. D. L., Wolf-Gladrow, D., Dürr, H., and
642 Scheffran, J.: Enhanced chemical weathering as a sink for carbon dioxide, a nutrient source
643 and a strategy to mitigate ocean acidification, *Reviews of Geophysics*, 2014b.

644 He Jiangyi, Z. D., Zhao zhiqi: Spatial and temporal variations in hydrochemical composition of
645 river water in Yellow River Basin, China, *Chinese Journal of Ecology*, 1-12, 2017.

646 Hercod, D. J., Brady, P. V., and Gregory, R. T.: Catchment-scale coupling between pyrite oxidation
647 and calcite weathering, *Chemical Geology*, 151, 259-276, [https://doi.org/10.1016/S0009-2541\(98\)00084-9](https://doi.org/10.1016/S0009-2541(98)00084-9), 1998.

649 Huh, Y., and Edmond, J. M.: The fluvial geochemistry of the rivers of Eastern Siberia: III.
650 Tributaries of the Lena and Anabar draining the basement terrain of the Siberian Craton and
651 the Trans-Baikal Highlands, *Geochimica et Cosmochimica Acta*, 63, 967-987,
652 [https://doi.org/10.1016/S0016-7037\(99\)00045-9](https://doi.org/10.1016/S0016-7037(99)00045-9), 1999.

653 Jiang, H., Liu, W., Xu, Z., Zhou, X., Zheng, Z., Zhao, T., Zhou, L., Zhang, X., Xu, Y., and Liu, T.:
654 Chemical weathering of small catchments on the Southeastern Tibetan Plateau I: Water sources,
655 solute sources and weathering rates, *Chemical Geology*, 500, 159-174,
656 <https://doi.org/10.1016/j.chemgeo.2018.09.030>, 2018.

657 Kempe, S., and Degens, E. T.: An early soda ocean?, *Chemical Geology*, 53, 95-108,
658 [https://doi.org/10.1016/0009-2541\(85\)90023-3](https://doi.org/10.1016/0009-2541(85)90023-3), 1985.

659 Khadka, M. B., Martin, J. B., and Jin, J.: Transport of dissolved carbon and CO₂ degassing from a
660 river system in a mixed silicate and carbonate catchment, *Journal of Hydrology*, 513, 391-402,
661 <https://doi.org/10.1016/j.jhydrol.2014.03.070>, 2014.

662 Larssen, T., and Carmichael, G. R.: Acid rain and acidification in China: the importance of base
663 cation deposition, *Environmental Pollution*, 110, 89-102, [https://doi.org/10.1016/S0269-7491\(99\)00279-1](https://doi.org/10.1016/S0269-7491(99)00279-1), 2000.

665 Larssen, T., Lydersen, E., Tang, D., He, Y., Gao, J., Liu, H., Duan, L., Seip, H. M., Vogt, R. D.,
666 Mulder, J., Shao, M., Wang, Y., Shang, H., Zhang, X., Solberg, S., Aas, W., Okland, T.,
667 Eilertsen, O., Angell, V., Li, Q., Zhao, D., Xiang, R., Xiao, J., and Luo, J.: Acid Rain in China,
668 *Environmental Science & Technology*, 40, 418-425, [10.1021/es0626133](https://doi.org/10.1021/es0626133), 2006.

669 Lenton, T. M., and Britton, C.: Enhanced carbonate and silicate weathering accelerates recovery
670 from fossil fuel CO₂ perturbations, *Global Biogeochemical Cycles*, 20,
671 [10.1029/2005gb002678](https://doi.org/10.1029/2005gb002678), 2006.

672 Li, R., Tang, C., Cao, Y., Jiang, T., and Chen, J.: The distribution and partitioning of trace metals
673 (Pb, Cd, Cu, and Zn) and metalloid (As) in the Beijiang River, *Environmental Monitoring and
674 Assessment*, 190, 399, [10.1007/s10661-018-6789-x](https://doi.org/10.1007/s10661-018-6789-x), 2018.

675 Li, R., Tang, C., Li, X., Jiang, T., Shi, Y., and Cao, Y.: Reconstructing the historical pollution levels
676 and ecological risks over the past sixty years in sediments of the Beijiang River, South China,
677 *Science of The Total Environment*, 649, 448-460,
678 <https://doi.org/10.1016/j.scitotenv.2018.08.283>, 2019.

679 Li, S. L., Calmels, D., Han, G., Gaillardet, J., and Liu, C. Q.: Sulfuric acid as an agent of carbonate
680 weathering constrained by $\delta^{13}\text{C}_{\text{DIC}}$: Examples from Southwest China, *Earth and Planetary
681 Science Letters*, 270, 189-199, <https://doi.org/10.1016/j.epsl.2008.02.039>, 2008.

682 Li, S., Lu, X. X., He, M., Zhou, Y., Bei, R., Li, L., and Ziegler, A. D.: Major element chemistry in
683 the upper Yangtze River: A case study of the Longchuanjiang River, *Geomorphology*, 129, 29-

684 42, <https://doi.org/10.1016/j.geomorph.2011.01.010>, 2011.

685 Li, S., Lu, X. X., and Bush, R. T.: Chemical weathering and CO₂ consumption in the Lower Mekong
686 River, *Science of The Total Environment*, 472, 162-177,
687 <https://doi.org/10.1016/j.scitotenv.2013.11.027>, 2014.

688 Liu, B., Liu, C.-Q., Zhang, G., Zhao, Z.-Q., Li, S.-L., Hu, J., Ding, H., Lang, Y.-C., and Li, X.-D.:
689 Chemical weathering under mid- to cool temperate and monsoon-controlled climate: A study
690 on water geochemistry of the Songhuajiang River system, northeast China, *Applied
691 Geochemistry*, 31, 265-278, <https://doi.org/10.1016/j.apgeochem.2013.01.015>, 2013.

692 Liu, Z., Dreybrodt, W., and Liu, H.: Atmospheric CO₂ sink: Silicate weathering or carbonate
693 weathering?, *Applied Geochemistry*, 26, S292-S294,
694 <https://doi.org/10.1016/j.apgeochem.2011.03.085>, 2011.

695 Liu, Z., and Dreybrodt, W.: Significance of the carbon sink produced by H₂O–carbonate–CO₂–
696 aquatic phototroph interaction on land, *Science Bulletin*, 60, 182-191, 2095-9273, 2015.

697 Ludwig, W., Amiotte-Suchet, P., Munhoven, G., and Probst, J.-L.: Atmospheric CO₂ consumption
698 by continental erosion: present-day controls and implications for the last glacial maximum,
699 *Global and Planetary Change*, 16-17, 107-120, [https://doi.org/10.1016/S0921-8181\(98\)00016-](https://doi.org/10.1016/S0921-8181(98)00016-2)
700 2, 1998.

701 Meybeck, M., Dürr, H. H., and Vörösmarty, C. J.: Global coastal segmentation and its river
702 catchment contributors: A new look at land-ocean linkage, *Global Biogeochemical Cycles*, 20,
703 10.1029/2005gb002540, 2006.

704 Mora, A., Baquero, J. C., Alfonso, J. A., Pisapia, D., and Balza, L.: The Apure River: geochemistry
705 of major and selected trace elements in an Orinoco River tributary coming from the Andes,
706 *Venezuela, Hydrological Processes*, 24, 3798-3810, 10.1002/hyp.7801, 2010.

707 Mortatti, J., and Probst, J.-L.: Silicate rock weathering and atmospheric/soil CO₂ uptake in the
708 Amazon basin estimated from river water geochemistry: seasonal and spatial variations,
709 *Chemical Geology*, 197, 177-196, [https://doi.org/10.1016/S0009-2541\(02\)00349-2](https://doi.org/10.1016/S0009-2541(02)00349-2), 2003.

710 Négrel, P., Allègre, C. J., Dupré, B., and Lewin, E.: Erosion sources determined by inversion of
711 major and trace element ratios and strontium isotopic ratios in river water: The Congo Basin
712 case, *Earth and Planetary Science Letters*, 120, 59-76, [https://doi.org/10.1016/0012-](https://doi.org/10.1016/0012-821X(93)90023-3)
713 821X(93)90023-3, 1993.

714 Ollivier, P., Hamelin, B., and Radakovitch, O.: Seasonal variations of physical and chemical erosion:
715 A three-year survey of the Rhone River (France), *Geochimica et Cosmochimica Acta*, 74, 907-
716 927, <https://doi.org/10.1016/j.gca.2009.10.037>, 2010.

717 Pike, R. J., and WILSON, S. E.: Elevation-Relief Ratio, Hypsometric Integral, and Geomorphic
718 Area-Altitude Analysis, *GSA Bulletin*, 82, 1079-1084, 10.1130/0016-
719 7606(1971)82[1079:erhiag]2.0.co;2, 1971.

720 Ran, X., Yu, Z., Yao, Q., Chen, H., and Mi, T.: Major ion geochemistry and nutrient behaviour in
721 the mixing zone of the Changjiang (Yangtze) River and its tributaries in the Three Gorges
722 Reservoir, *Hydrological processes*, 24, 2481-2495, 2010.

723 Rao, W., Zheng, F., Tan, H., Yong, B., Jin, K., Wang, S., Zhang, W., Chen, T., and Wang, Y.: Major
724 ion chemistry of a representative river in South-central China: Runoff effects and controlling
725 mechanisms, *Journal of Hazardous Materials*, 378, 120755,
726 <https://doi.org/10.1016/j.jhazmat.2019.120755>, 2019.

727 Ryu, J. S., Lee, K. S., Chang, H.-W., and Shin, H. S.: Chemical weathering of carbonates and

728 silicates in the Han River basin, South Korea, *Chemical Geology*, 247, 66-80,
729 <https://doi.org/10.1016/j.chemgeo.2007.09.011>, 2008.

730 Singh, O., Sarangi, A., and Sharma, M. C.: Hypsometric Integral Estimation Methods and its
731 Relevance on Erosion Status of North-Western Lesser Himalayan Watersheds, *Water*
732 *Resources Management*, 22, 1545-1560, 10.1007/s11269-008-9242-z, 2008.

733 Spence, J., and Telmer, K.: The role of sulfur in chemical weathering and atmospheric CO₂ fluxes:
734 Evidence from major ions, $\delta^{13}\text{C}_{\text{DIC}}$, and $\delta^{34}\text{S}_{\text{SO}_4}$ in rivers of the Canadian Cordillera,
735 *Geochimica et Cosmochimica Acta*, 69, 5441-5458, <https://doi.org/10.1016/j.gca.2005.07.011>,
736 2005.

737 Stallard, R. F., and Edmond, J. M.: Geochemistry of the Amazon: 1. Precipitation chemistry and the
738 marine contribution to the dissolved load at the time of peak discharge, *Journal of Geophysical*
739 *Research: Oceans*, 86, 9844-9858, 10.1029/JC086iC10p09844, 1981.

740 Stallard, R. F., and Edmond, J. M.: Geochemistry of the Amazon: 2. The influence of geology and
741 weathering environment on the dissolved load, *Journal of Geophysical Research: Oceans*, 88,
742 9671-9688, 10.1029/JC088iC14p09671, 1983.

743 Stallard, R. F., and Edmond, J. M.: Geochemistry of the Amazon: 3. Weathering chemistry and limits
744 to dissolved inputs, *Journal of Geophysical Research: Oceans*, 92, 8293-8302,
745 10.1029/JC092iC08p08293, 1987.

746 STRAHLER, A. N.: HYPSONOMETRIC (AREA-ALTITUDE) ANALYSIS OF EROSIONAL
747 TOPOGRAPHY, *GSA Bulletin*, 63, 1117-1142, 10.1130/0016-
748 7606(1952)63[1117:haoet]2.0.co;2, 1952.

749 Sun, X., Mörth, C.-M., Humborg, C., and Gustafsson, B.: Temporal and spatial variations of rock
750 weathering and CO₂ consumption in the Baltic Sea catchment, *Chemical Geology*, 466, 57-69,
751 <https://doi.org/10.1016/j.chemgeo.2017.04.028>, 2017.

752 Taylor, B. E., Wheeler, M. C., and Nordstrom, D. K.: Stable isotope geochemistry of acid mine
753 drainage: Experimental oxidation of pyrite, *Geochimica et Cosmochimica Acta*, 48, 2669-2678,
754 [https://doi.org/10.1016/0016-7037\(84\)90315-6](https://doi.org/10.1016/0016-7037(84)90315-6), 1984.

755 Van Everdingen, R. O., and Krouse, H. R.: Isotope composition of sulphates generated by bacterial
756 and abiological oxidation, *Nature*, 315, 395-396, 10.1038/315395a0, 1985.

757 Viers, J., Oliva, P., Dandurand, J. L., Dupré, B., and Gaillardet, J.: Chemical weathering rates, CO₂
758 consumption, and control parameters deduced from the chemical composition of rivers, 2014.

759 Walling, D. E.: Solute in river systems, *Solute Processes*, 251-327, 1986.

760 Wen, J., Tang, C., Cao, Y., Li, X., and Chen, Q.: Hydrochemical evolution of groundwater in a
761 riparian zone affected by acid mine drainage (AMD), South China: the role of river-
762 groundwater interactions and groundwater residence time, *Environmental Earth Sciences*, 77,
763 794, 10.1007/s12665-018-7977-2, 2018.

764 Wu, W., Xu, S., Yang, J., and Yin, H.: Silicate weathering and CO₂ consumption deduced from the
765 seven Chinese rivers originating in the Qinghai-Tibet Plateau, *Chemical Geology*, 249, 307-
766 320, 2008.

767 Xie chenji, G. Q., Tao zhen, Liu Longhai, Lishanchi: Chemical weathering and CO₂ consumption
768 in the Dongjiang River Basin, *Acta Scientiae Circumstantiae*, 33, 2123-2133, 2013.

769 Xiong, L., Tang, G., Yuan, B., Lu, Z., Li, F., and Zhang, L.: Geomorphological inheritance for loess
770 landform evolution in a severe soil erosion region of Loess Plateau of China based on digital
771 elevation models, *Science China Earth Sciences*, 57, 1944-1952, 10.1007/s11430-014-4833-4,

772 2014.

773 Xu, Z., and Liu, C.-Q.: Water geochemistry of the Xijiang basin rivers, South China: Chemical
774 weathering and CO₂ consumption, *Applied Geochemistry*, 25, 1603-1614, 2010.

775 Zeng, C., Liu, Z., Zhao, M., and Yang, R.: Hydrologically-driven variations in the karst-related
776 carbon sink fluxes: Insights from high-resolution monitoring of three karst catchments in
777 Southwest China, *Journal of Hydrology*, 533, 74-90,
778 <https://doi.org/10.1016/j.jhydrol.2015.11.049>, 2016.

779 Zhang, J., Huang, W., Letolle, R., and Jusserand, C.: Major element chemistry of the Huanghe
780 (Yellow River), China-weathering processes and chemical fluxes, *Journal of Hydrology*, 168,
781 173-203, 1995.

782 Zhang, L., Song, X., Xia, J., Yuan, R., Zhang, Y., Liu, X., and Han, D.: Major element chemistry of
783 the Huai River basin, China, *Applied Geochemistry*, 26, 293-300, 2011.

784 Zhang, S. R., Lu, X. X., Higgitt, D. L., Chen, C. T. A., Sun, H. G., and Han, J. T.: Water chemistry
785 of the Zhujiang (Pearl River): natural processes and anthropogenic influences. *Journal of*
786 *Geophysical Research*, 112(F1), F01011, *Journal of Geophysical Research Atmospheres*, 112,
787 137-161, 2007.

788 **Supplementary material**

789 **Table S1 The major ions concentrations of rain water samples at 5 hydrological stations in the**

790 **Beijiang River (mean±SD).**

Hydrological stations	Na ⁺ (μmol/L)	K ⁺ (μmol/L)	Ca ²⁺ (μmol/L)	Mg ²⁺ (μmol/L)	Cl ⁻ (μmol/L)	SO ₄ ²⁻ (μmol/L)	NO ₃ ⁻ (μmol/L)
XGLs	12.8±9.7	21.0±16.8	22.2±20.5	10.9±10.3	25.9±22.6	320.2±370.7	83.3±85.2
XSs	20.4±11.8	7.8±4.5	86.9±30.4	10.1±5.2	10.0±0.0	606.5±511.5	36.3±23.4
Yds	16.3±9.5	10.1±10.8	161.1±56.5	9.0±7.8	23.9±12.4	136.9±169.5	143.1±135.5
FLXs	18.8±12.3	3.2±2.5	31.1±17.7	4.2±2.7	23.1±16.6	45.4±27.5	77.1±70.4
SJs	12.6±9.2	12.5±16.3	22.9±13.8	15.4±18.1	25.4±16.0	79.0±79.8	156.7±206.4

791